https://doi.org/10.5194/egusphere-2026-5226
Preprint. Discussion started: 9 September 2026

URAY v1.0: a 3D Monte Carlo model for urban shortwave radiation with explicit buildings and tree canopies

Shuo-Jun Mei[1,3], Zhanmin Wu[1], Jiang-Tao Hu[2,3], Taihan Chen[4], Guanwen Chen[1,3], and Ting Sun[5]

[1]School of Atmospheric Sciences, Sun Yat-sen University, and Southern Marine Science and Engineering Guangdong Laboratory (Zhuhai), Zhuhai 519082, PR China
[2]School of Automation, Guangdong Polytechnic Normal University, Guangzhou, PR China
[3]China Meteorological Administration Xiong'an Atmospheric Boundary Layer Key Laboratory, Xiong'an, PR China
[4]National University of Singapore, Singapore
[5]Department of Risk and Disaster Reduction, University College London, London, UK

Correspondence: Guanwen Chen (chengw67@mail.sysu.edu.cn)

Abstract. Urban canopy models with trees often represent radiation exchange with idealized street canyon geometry. These models clarify tree shading, canopy interception, and multiple reflection, but they cannot directly resolve the 3D arrangement of buildings and tree crowns across real city districts. URAY addresses this limitation as a city-scale 3D Monte Carlo model for urban shortwave radiative transfer that resolves both buildings and tree crowns. The model extends a building-resolving shortwave solver by adding ellipsoidal tree crowns as transmissive participating media, Woodcock tracking for stochastic canopy interactions, bounding volume hierarchy (BVH) acceleration for complex urban meshes, and GPU parallel photon tracing. The coupled framework resolves explicit building surfaces and tree crowns in one 3D radiative transfer domain and diagnoses both scene albedo and absorbed shortwave radiation for ground, walls, roofs, and tree canopies. Two validation experiments test the canopy transmissivity formulation and the coupled building–tree albedo response in a 3D urban block. URAY reproduces the observed radiative behavior in both cases. We then apply URAY to Guangzhou, a subtropical city with high building density and dense urban tree cover, using resolved 3D building and canopy geometry. This city-scale simulation demonstrates that GPU-parallel URAY can efficiently resolve component-level shortwave absorption across an entire city.

1 Introduction

Urban shortwave radiation is a central control on urban surface energy balance. Increasing roof and pavement albedo has widely been proposed as a strategy to modify urban shortwave radiative forcing (Akbari et al., 2009; Menon et al., 2010; Yang et al., 2015). However, the effectiveness of this strategy depends on the geometric context of urban surfaces, which can trap radiation and reduce effective albedo relative to a flat surface of the same material (Aida and Gotoh, 1982; Arnfield, 1982). Additionally, urban trees modify shortwave redistribution through shading, interception, absorption, transmission, and scattering (Krayenhoff et al., 2014; Meili et al., 2020; Wang et al., 2021). The net effect of trees on urban albedo is therefore not only a function of tree density and leaf optical properties, but also of the geometric arrangement of buildings and tree crowns.

https://doi.org/10.5194/egusphere-2026-5226
Preprint. Discussion started: 9 September 2026

The dependence of building geometry has been recognized since early urban canyon studies. Scale model experiments and 2D numerical simulations showed that urban structures can trap solar radiation and reduce effective albedo relative to a horizontal surface of the same material (Aida and Gotoh, 1982). Subsequent radiation budget models formalized the roles of direct and diffuse shortwave reflection, longwave exchange, and multiple reflection in urban canyon forms (Arnfield, 1982, 1988). Later studies extended this line of work to diurnal effective albedo, cool pavement applications, and canyon albedo calculations under direct and diffuse radiation (Sailor and Fan, 2002; Fortuniak, 2008; Qin, 2015; Salvati et al., 2022). Together these studies establish that canyon aspect ratio, solar angle, wall and road reflectance, and exchange between surfaces all control the apparent albedo of urban fabric. However, many of these formulations are still based on idealized 2D canyons, regular arrays, or reduced view factor calculations.

Urban trees amplify the mismatch between 2D canyon assumptions and the geometric complexity of real urban scenes. Trees are widely used in urban design, yet their shortwave radiative role extends beyond shading. They reduce irradiance on ground and walls, but they also intercept, absorb, transmit, and scatter sunlight, thereby modifying both apparent urban albedo and the internal redistribution of absorbed shortwave energy. A scene with trees exhibits higher albedo when canopy scattering increases upward shortwave flux, and lower albedo when additional solar energy is trapped and absorbed within the canopy. Either outcome can still coincide with reduced loading on hard surfaces if absorption is shifted away from ground and walls. For urban climate applications, the key question is therefore not only whether trees raise or lower albedo, but also where the redirected energy is ultimately absorbed.

Several urban canopy models have introduced trees into this radiation problem, but most remain tied to 2D street canyon geometry. Radiation models for urban neighbourhoods with multiple vertical layers and trees have used ray tracing and Monte Carlo view factor calculations to represent interactions between trees and radiation (Krayenhoff et al., 2014). UT&C represents urban vegetation, water balance, and energy exchange in an infinite canyon framework and computes tree effects through canyon scale radiation, hydrological, and physiological processes (Meili et al., 2020). More recently, a single layer urban canopy model (SLUCM) introduced transmissive radiation exchange between trees and street canyons (Wang et al., 2021). These studies demonstrate that urban vegetation is represented more physically as a transmissive and absorbing medium than as an opaque block. However, these models still rely on idealized canyon geometry. Consequently, they cannot directly resolve finite building layouts, irregular tree placement, crown overlap, roof and wall exposure, or the spatial heterogeneity of real 3D city districts.

Models for 3D radiative transfer have improved urban radiation representation by resolving complex geometry and calculating radiative exchange with Monte Carlo or ray-tracing methods. Panao et al. (2007) coupled matrix radiosity with Monte Carlo techniques to estimate view factors and solve the net radiative balance of an urban block. Manni et al. (2020) developed and validated a Monte Carlo numerical model to analyse solar radiation in urban canyon configurations. Overby et al. (2016) used GPU-accelerated ray tracing to simulate radiation transfer across complex urban domains at practical runtimes. Villefranque et al. (2022) formulated urban radiative and heat transfer as a Monte Carlo path-integral problem, enabling complex urban geometry to be represented without reduction to canonical facets. Caliot et al. (2024) applied this Monte Carlo formulation to resolve coupled heat transfer in urban geometry under direct and diffuse solar irradiance. Schoetter et al. (2023) compared

https://doi.org/10.5194/egusphere-2026-5226
Preprint. Discussion started: 9 September 2026

urban canopy radiative-transfer calculations to quantify how model approximations propagate into uncertainty in calculated radiation budgets. Landier et al. (2018) combined remote-sensing data with the DART model to calibrate urban canopy albedo and reconstruct three-dimensional shortwave radiation budgets. Wang et al. (2024) extended DART with three-dimensional Monte Carlo surface–atmosphere radiative transfer to simulate coupled radiation propagation through urban surfaces and the atmosphere. These developments demonstrate Monte Carlo ray tracing as a strong methodological basis for urban radiative transfer modelling. However, combining city-scale execution, explicit building geometry, resolved transmissive tree crowns, and component-level shortwave absorption diagnostics in one workflow remains technically demanding. This combination is especially relevant in high-density subtropical Asian cities where compact urban form and extensive tree cover jointly shape shortwave redistribution.

To address this gap, Mei et al. (2025) introduced a shortwave solver for resolved buildings based on three-dimensional urban morphology. The current URAY builds on that solver and extends it to a city-scale radiative transfer framework that includes both buildings and trees. The model no longer relies on a 2D street canyon or on a reduced set of bulk morphological parameters. Instead, it represents urban surfaces as explicit triangulated geometry, treats resolved ellipsoidal tree crowns as participating media, applies Woodcock tracking for stochastic canopy interactions, accelerates building and ray intersections with a bounding volume hierarchy (BVH), and traces photons in parallel on the GPU. This design allows scene albedo to be diagnosed together with absorbed shortwave radiation by ground, wall, roof, and canopy components. The Guangzhou application demonstrates how the validated model computes urban area albedo and ground absorption ratio from explicit 3D building and canopy geometry in a subtropical city with high building density, abundant trees, and strong neighbourhood-scale morphology contrasts.

The manuscript are organized as follows. First, Section 2 describes the model development, including the city-scale implementation framework, Monte Carlo ray tracing for urban surfaces, tree transmissivity and Woodcock tracking, BVH acceleration and GPU parallelization, and the Guangzhou application. Second, Section 3 presents two validation experiments that test the canopy transmissivity formulation and the coupled building–tree albedo response in a 3D urban block. Third, Section 4 presents the Guangzhou application, including city-scale albedo and absorbed shortwave radiation diagnostics, morphology-stratified analysis, and the role of trees in modifying shortwave redistribution. Finally, Section 5 summarizes the advances and limitations of URAY.

2 Model development

2.1 City-scale implementation framework from GIS data

Figure 1 summarizes the framework for implementing URAY at city scale. The workflow begins by dividing city-scale GIS layers into approximately kilometre-scale tiles containing building footprints and heights, tree cover, and tree canopy height data. In the Guangzhou application, the building footprint and height information is taken from the 3D-GloBFP global three-dimensional building footprint dataset (Che et al., 2024), while the tree canopy layer is derived from the very high resolution global canopy height product of Tolan et al. (2024). For each tile, the building footprints, building heights, and canopy height

https://doi.org/10.5194/egusphere-2026-5226
Preprint. Discussion started: 9 September 2026

information are transferred from GIS into a three-dimensional model in which buildings are represented as explicit surface geometry and tree crowns are represented as ellipsoids. These three-dimensional surfaces and crown objects form the ray-tracing domain used by URAY. The model is then forced with solar geometry and shortwave radiation data, executed tile by tile with the URAY solver, and mapped back to GIS space to diagnose scene albedo and absorbed shortwave radiation by component.

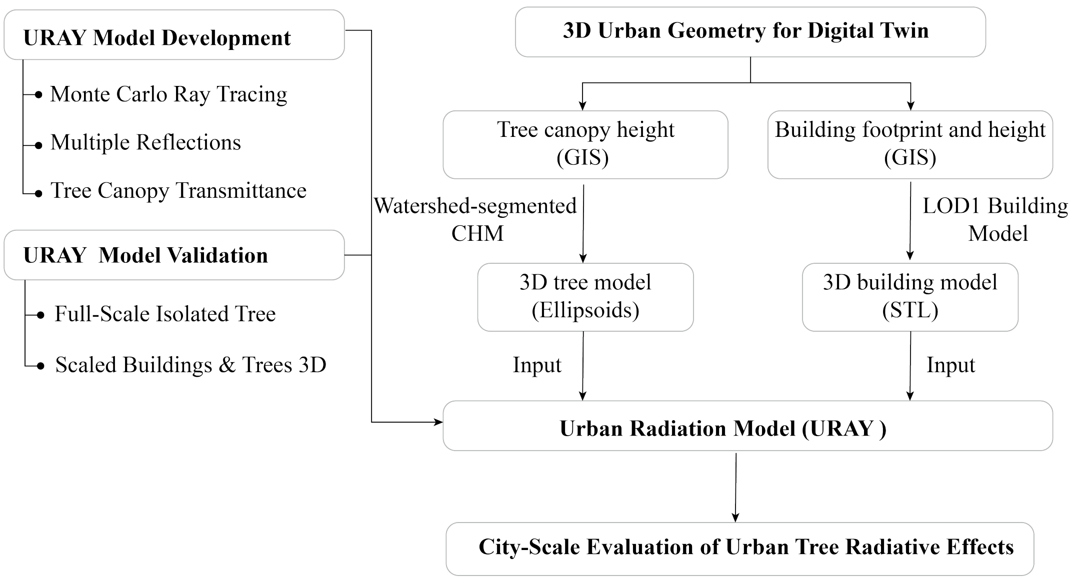

Figure 1. City-scale workflow of URAY with resolved buildings and tree crowns. Building footprints and building heights from 3D-GloBFP (Che et al., 2024), together with tree canopy height data derived from Tolan et al. (2024), are converted into explicit 3D building surfaces and resolved crown objects for urban shortwave radiative transfer simulation. The framework couples Monte Carlo ray tracing for buildings with transmissive radiative transfer through tree canopies, allowing scene albedo and absorbed shortwave radiation by ground, wall, roof, and canopy components to be evaluated from validation cases to city-scale Guangzhou applications.

URAY calculates shortwave radiation by tracing photons through urban surfaces, which requires explicit 3D geometry for buildings and tree crowns. Figure 2 shows the preprocessing workflow that converts GIS building and tree layers into a format suitable for ray tracing. The workflow converts a $1\,\mathrm{km} \times 1\,\mathrm{km}$ tile in Guangzhou into a 3D model suitable for ray tracing. The process of building geometry generation and tree canopy generation is handled separately, as the former produces explicit surface meshes while the latter produces compact ellipsoidal crown objects for participating media.

Building footprints and heights are converted to an STL urban surface model with explicit wall, roof, and ground classes. The polygons are transformed to a metric projected coordinate system when needed, shifted to a local origin, filtered to remove very small patches, and simplified to convex hull footprints before extrusion. For each footprint edge, the preprocessing workflow calculates an outward horizontal normal so that wall facets retain a consistent orientation in the exported mesh. The workflow then writes an STL in which walls, roofs, and the background ground plane are stored as separate named solids, allowing URAY to ingest the city scene as a triangulated urban mesh and accumulate absorbed shortwave radiation by surface class.

https://doi.org/10.5194/egusphere-2026-5226
Preprint. Discussion started: 9 September 2026

Tree canopies are converted from raster-derived crown segments to analytic ellipsoids described by crown centre coordinates, horizontal and vertical semi-axis lengths, leaf area density (LAD), and a leaf angle distribution parameter χ . The tree pipeline smooths the canopy height raster with a Gaussian filter, detects tree tops through a local maximum search, and applies watershed segmentation on the inverted canopy surface to delineate individual crowns. Each segmented crown is exported as a polygon for GIS checking and then converted to one ellipsoid whose horizontal radii are inferred from the crown footprint and whose vertical radius is set from crown height. The resulting tree table stores the ellipsoid centre coordinates, semi-axis lengths, and canopy radiative parameters required by URAY.

This design allows the city-scale workflow to preserve explicit building surfaces while representing trees in a compact form for participating media that remains computationally feasible for large numbers of tiles. The resulting STL meshes and tree CSV files are then read by the URAY solver for each tile, which computes scene albedo and absorbed shortwave radiation by ground, wall, roof, and canopy components. The outputs are then mapped back to GIS space to produce city-scale diagnostics of how trees modify shortwave budgets in real urban scenes.

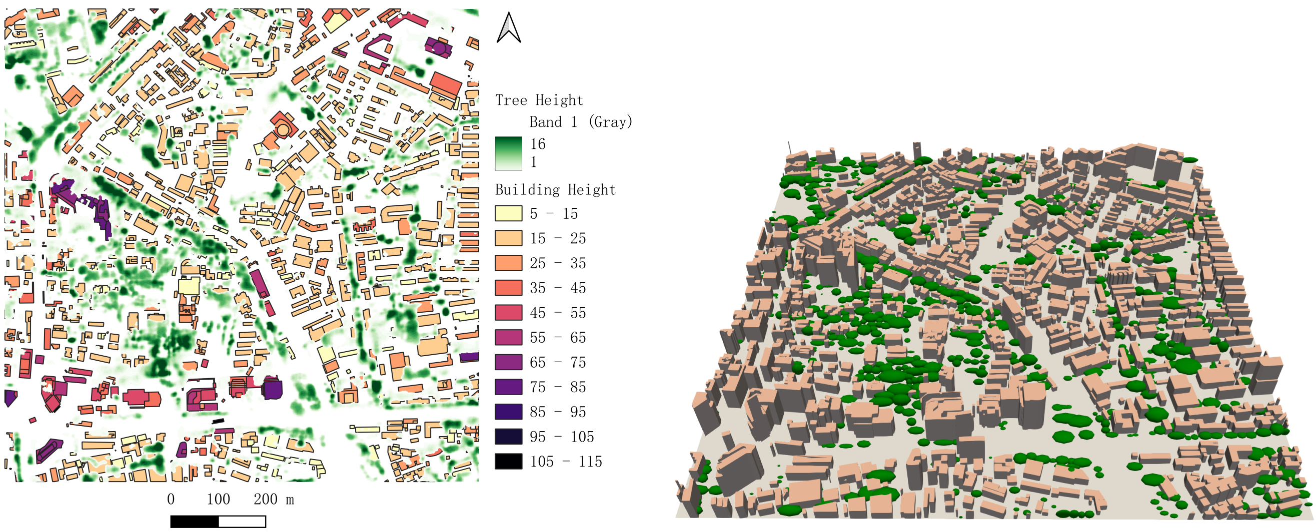

(a) GIS building and tree height inputs

(b) Generated three-dimensional scene

Figure 2. Generation of the three-dimensional building and canopy geometry for a representative Guangzhou simulation tile. Panel (a) shows the source GIS layers, with building height represented by footprint polygons and tree height represented by the canopy height raster. Panel (b) shows the corresponding URAY scene after buildings are extruded into wall and roof surfaces and tree crowns are converted into volumetric ellipsoids.

2.2 Monte Carlo ray tracing for urban surfaces

URAY inherits the urban shortwave solver with resolved buildings from Mei et al. (2025). Urban surfaces are represented explicitly as triangulated meshes, and direct and diffuse solar radiation are simulated with forward Monte Carlo ray tracing. Buildings are imported from STL and split into wall, roof, and ground surfaces by reading named solids from the geometry

https://doi.org/10.5194/egusphere-2026-5226
Preprint. Discussion started: 9 September 2026

file. Each surface is stored as a triangle mesh with outward unit normals, and the GPU kernels track index ranges for each surface class so that absorbed energy can be accumulated independently by component. Surface reflectance is determined by the albedo assigned to each surface class (e.g., walls, roofs, and ground surfaces). In the current version, the base albedo can also be adjusted for solar incidence angle using a correction based on `pvlib` in the preprocessing workflow (Holmgren et al., 2018).

Figure 3 illustrates the core ray tracing design used by URAY. The model traces direct and diffuse solar photons through urban canyons containing explicit building surfaces and participating tree crowns. Building facets are treated as opaque reflecting and absorbing boundaries: when a ray intersects a ground, wall, or roof triangle, the photon is either absorbed by that surface class or reflected back into the urban scene. Tree crowns are treated differently, as transmissive ellipsoidal volumes. A ray that enters a crown is not stopped at the ellipsoid boundary; instead, it travels through the crown volume, where absorption, scattering, null collisions, or complete transmission are sampled along the internal path. Building intersections are accelerated with a bounding volume hierarchy (BVH), while photon transport inside tree crowns is handled with Woodcock tracking so that scattering, absorption, null collisions, and continued transmission can be sampled stochastically along the ray path.

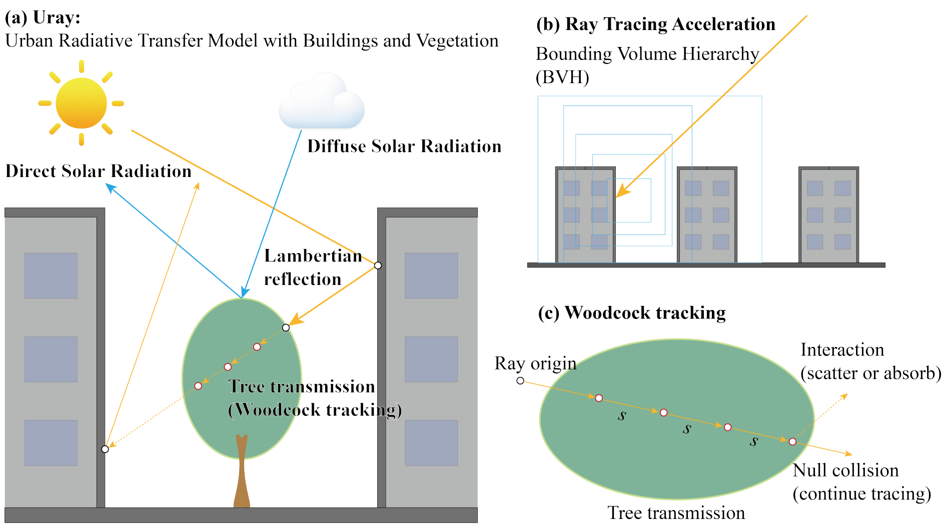

Figure 3. Schematic of the URAY photon tracing framework. Panel (a) shows the coupled urban radiative transfer problem with direct and diffuse solar radiation, Lambertian surface reflection, and transmission through tree canopies. Panel (b) illustrates BVH acceleration for ray tracing in building geometry. Panel (c) shows the Woodcock tracking path used to sample stochastic photon interactions inside a participating tree crown.

Following the formulation of Mei et al. (2025), each photon is launched from a random point on the upper boundary of the computational domain. As shown in Figure 3 (a), direct photons follow the solar vector, while diffuse photons are emitted from the same top plane with a sampled downward hemispherical direction. The ray is then marched through the scene until it is absorbed. If the ray leaves the top of the domain, reaches the maximum reflection count used in the kernel, the marching process is interrupted. At building surfaces, this marching process is interrupted by the absorption and reflection test described

https://doi.org/10.5194/egusphere-2026-5226
Preprint. Discussion started: 9 September 2026

below. At tree crowns, the ray first intersects the ellipsoid entry and exit points and then propagates through the participating volume between those points, so transmission through the crown is represented as a path process rather than as a binary shadow. Lateral boundary crossings are treated periodically by moving the photon to the opposite side of the tile, allowing a finite tile to approximate a repeating urban fabric.

At every surface hit, URAY performs a stochastic absorption–reflection test. Let ρ_j be the reflectance assigned to the intersected surface class j, where $j \in \{g, w, r\}$ denotes ground, wall, and roof. A uniform random number $R_1 \in [0,1]$ is generated. If $R_1 > \rho_j$, the photon is absorbed by that surface class and the photon history terminates. If $R_1 \leq \rho_j$, the photon is reflected and continues to the next interaction. This event-based accounting is the basis for both scene albedo and the absorbed shortwave partition among urban surface classes.

Surface reflection is treated as Lambertian. Two additional random numbers, R_2 and R_3, are used to sample a reflected direction over the hemisphere oriented by the local surface normal:

$$\varphi = 2\pi R_2, \tag{1}$$

$$\eta = \arccos\sqrt{1 - R_3}, \tag{2}$$

where φ is the azimuthal angle and η is the polar angle from the surface normal. This sampled vector is rotated from the local upward hemisphere to the hit triangle normal and then used as the new ray direction. Because reflected photons remain active until absorption or escape, multiple reflection and radiation trapping among ground, walls, roofs, and tree crowns are represented explicitly rather than through view-factor closure.

For each radiation component and time step, URAY records whether each photon is absorbed by ground, wall, or roof. If F_j^o and F_j^d are the numbers of direct and diffuse photons absorbed by surface class j, and N is the number of photons traced for each component, then the direct and diffuse absorption ratios are

$$A_j^o = \frac{F_j^o}{N}, \qquad A_j^d = \frac{F_j^d}{N}. \tag{3}$$

Here $j = g, w, r$ denotes ground, wall, and roof, so A_g^o, A_w^o, and A_r^o are the direct-beam fractions absorbed by ground, wall, and roof, while A_g^d, A_w^d, and A_r^d are the corresponding diffuse-sky fractions. The returned instantaneous surface absorption ratios are

$$A_g = \frac{A_g^o I_o + A_g^d I_d}{I_o + I_d}, \qquad A_w = \frac{A_w^o I_o + A_w^d I_d}{I_o + I_d}, \qquad A_r = \frac{A_r^o I_o + A_r^d I_d}{I_o + I_d}. \tag{4}$$

These quantities are dimensionless fractions of the incident shortwave forcing absorbed by each urban surface class during the simulated time step.

The corresponding direct and diffuse albedos are computed from the numbers of photons that do not escape the upper boundary. Let Q^o and Q^d be the direct and diffuse photon counts that terminate by absorption in either an urban surface or a tree crown. Then

$$\alpha_o = 1 - \frac{Q^o}{N}, \qquad \alpha_d = 1 - \frac{Q^d}{N}. \tag{5}$$

https://doi.org/10.5194/egusphere-2026-5226
Preprint. Discussion started: 9 September 2026

The same direct and diffuse shortwave components are then used to combine the two photon ensembles for scene albedo:

$$\alpha = \frac{\alpha_o I_o + \alpha_d I_d}{I_o + I_d}, \tag{6}$$

$$A_j = \frac{A_j^o I_o + A_j^d I_d}{I_o + I_d}. \tag{7}$$

The compact form A_j is used when referring to any one of the three surface classes. The daylight summary used in the tile tables is then calculated from the sunlit hourly records, for example

$$\overline{\alpha}^{\text{day}} = \frac{1}{N_{\text{day}}} \sum_{t \in \mathcal{D}} \alpha(t), \qquad \overline{A_g}^{\text{day}} = \frac{1}{N_{\text{day}}} \sum_{t \in \mathcal{D}} A_g(t), \tag{8}$$

where $\mathcal{D}$ is the set of time steps with positive downward shortwave forcing and N_{day} is the number of such time steps. The wall and roof daylight absorption summaries are calculated in the same way.

2.3 Tree transmissivity and Woodcock tracking

Trees are introduced as transmissive participating media rather than opaque shading objects. Each crown is represented as an idealized ellipsoid defined by centre coordinates (x, y, z), semi-axis lengths (r_x, r_y, r_z), leaf area density (LAD), and a directional foliage projection parameter χ. The tree list is read from CSV and converted into an array of analytic crown objects. This compact representation is suitable for large urban scenes while preserving the first order canopy controls required for attenuation, scattering, and transmission.

For each photon, the solver finds the nearest urban triangle, the nearest tree crown intersection, and the nearest lateral boundary event. If a crown is encountered before an urban surface, analytic ray and ellipsoid intersection gives the entry and exit distances through the crown. In the absence of an accepted interaction, the photon is transmitted through the crown and continues through the urban scene. This means canopy transmissivity emerges from crown path length, LAD, and leaf angle rather than being imposed as a fixed shading factor.

Stochastic interactions inside the crown are sampled with Woodcock tracking, also known as delta tracking. As shown in Figure 3 (c), after the ray is advanced to the ellipsoid entry point, the available path length inside the crown is

$$L_{\text{crown}} = t_{\text{exit}} - t_{\text{entry}}. \tag{9}$$

Candidate collision distances are sampled from an exponential free-path distribution using a majorant extinction coefficient $\sigma_{\max}$:

$$\Delta s = -\frac{\ln R_0}{\sigma_{\max}}, \tag{10}$$

where $R_0 \in (0, 1]$ is a uniform random number. The cumulative distance inside the crown is updated as $s \leftarrow s + \Delta s$. If $s \geq L_{\text{crown}}$, no canopy interaction occurs before the ray leaves the ellipsoid, and the photon is transmitted to the exit point. If $s < L_{\text{crown}}$, the candidate point is treated as a canopy collision. In the present homogeneous ellipsoid implementation, $\sigma_{\max} = \sigma_t$, so every candidate collision is accepted. More generally, for a spatially varying crown extinction field, a candidate event would

https://doi.org/10.5194/egusphere-2026-5226
Preprint. Discussion started: 9 September 2026

be accepted with probability $\sigma_t/\sigma_{\max}$, and otherwise treated as a null collision. Within the crown, the extinction coefficient is evaluated as

$$\sigma_t = \mathrm{LAD}\,G(\theta), \tag{11}$$

where $G(\theta)$ is evaluated from χ and the incoming ray direction.

At an accepted canopy event, a photon is absorbed with probability $1-\omega_{LD}$. Otherwise it is scattered, with a specular branch of probability ω_{LS}/ω_{LD} and a diffuse branch for the remainder. The scattered photon is then traced further so that canopy transmission, canopy absorption, and subsequent building interactions remain fully coupled. The probabilities ω_{LD} and ω_{LS} therefore control the leaf-scale non-absorption and scattering-direction partition used by the crown module. This approach avoids voxelizing the canopy or explicitly meshing individual leaves, while still allowing crown path length, LAD, and leaf angle projection to control stochastic transmission.

The canopy optical probabilities are linked to optical properties at leaf scale with a PROSPECT family leaf optical model (Jacquemoud and Baret, 1990; Feret et al., 2017). In the demonstration case, PROSPECT is run with a representative green broadleaf parameter set: leaf structure parameter $N = 2.0$, chlorophyll content $C_{ab} = 35$, carotenoid content $C_{ar} = 12$, brown pigment content $C_{brown} = 0.0$, equivalent water thickness $C_w = 0.01$, and dry matter content $C_m = 0.12$. The resulting leaf reflectance $\rho(\lambda)$ and transmittance $\tau(\lambda)$ spectra are averaged over the shortwave range 400–2500 nm, and the probability of a collision without absorption is estimated as

$$\omega_{LD} = \overline{\rho}_{400-2500} + \overline{\tau}_{400-2500}. \tag{12}$$

For the representative green broadleaf parameter set used here, this spectral averaging gives $\omega_{LD} = 0.80$, which is adopted as the baseline value in the validation and Guangzhou simulations. The second optical parameter, ω_{LS}, is not a direct PROSPECT output. It partitions the events that are not absorbed into a specular branch and a diffuse branch, and is therefore prescribed as an effective parameter for scattering direction. The validation and Guangzhou runs reported here use $\omega_{LS} = 0.30$ as a baseline effective value rather than as an independently measured leaf optical property. Thus $1-\omega_{LD}$, ω_{LS}, and $\omega_{LD}-\omega_{LS}$ represent the probabilities of canopy absorption, specular scattering, and diffuse scattering, respectively.

2.4 BVH acceleration, GPU parallelization, and output diagnostics

The main acceleration strategy for urban geometry is a bounding volume hierarchy (BVH). This acceleration is necessary because ray tracing at the neighbourhood scale, for example over a $1\,\mathrm{km}\times 1\,\mathrm{km}$ tile, can involve thousands to tens of thousands of building triangle surfaces. Testing every photon against every triangle would make the simulation prohibitively expensive. As shown in Figure 3b, a BVH is a tree of nested axis aligned bounding boxes: each internal node encloses a subset of triangles, and each leaf node stores only a small number of triangle indices. URAY builds the BVH over the full urban triangle set on the host before the time loop starts. Triangles are recursively partitioned by centroid position along the axis with the largest spatial extent until a maximum leaf size is reached. Each node stores its bounding-box minimum and maximum coordinates, child-node indices, or the start and count of the triangle indices contained in the leaf.

https://doi.org/10.5194/egusphere-2026-5226
Preprint. Discussion started: 9 September 2026

During photon tracing, the GPU kernel traverses this hierarchy with an explicit stack. A ray is first tested against bounding boxes, and triangle intersection tests are performed only for leaves whose boxes are intersected and whose entry distance is closer than the current closest hit. This replaces the brute-force search over all urban triangles with a hierarchical rejection process, which is critical for city tiles containing thousands to tens of thousands of wall and roof facets. Tree crowns are handled separately through analytic ellipsoid intersections, so the BVH exclusively accelerates the building surface part of the coupled workflow.

GPU parallelization follows the natural independence of Monte Carlo photon paths. The wrapper allocates one output slot per photon for direct and diffuse albedo contribution and for ground, wall, and roof absorption flags. It launches separate direct and diffuse CUDA kernels. Each thread tracks one photon history, including surface intersections, lateral periodic wrapping, Lambertian reflection, crown intersections, Woodcock events, absorption, and escape. After the kernels finish, the host sums the per photon arrays to obtain direct and diffuse albedo and component absorption ratios, then combines them with I_o and I_d. Because photon histories do not need communication during tracing, this strategy maps efficiently to the GPU and allows the city-scale batch workflow to retain explicit 3D geometry.

2.5 City-scale implementation

This section shows how URAY can be implemented at city scale, using Guangzhou as an example application. Guangzhou is suitable for this demonstration because districts with dense buildings, open residential neighbourhoods, and green areas coexist within the same regional climate, creating strong heterogeneity in both building morphology and canopy cover. Canopy cover is most continuous in the northern and northeastern parts of Guangzhou, where forested and hilly areas dominate, and is more fragmented across the central and southern urbanized corridor. In contrast, the building layer is densest in the central–western urban core and along the main developed corridor toward the south, while the northern and northeastern green areas contain much lower building density. This heterogeneity provides a representative testbed for evaluating how contrasting combinations of buildings and trees shape urban radiative exchange at the city scale.

The two city-scale GIS inputs used by URAY provide the structural context for this application. The tree input is a canopy height layer derived from the very high resolution canopy height map of Tolan et al. (2024), and the building input is a footprint and height layer from the 3D-GloBFP dataset of Che et al. (2024) (Figure 4). Together, these layers define the physical scene passed to the model: the building data determine the explicit wall, roof, and ground geometry, while the canopy height data determine the location and size of resolved tree crowns. The Guangzhou application comprises 6761 completed $1\ \mathrm{km} \times 1\ \mathrm{km}$ simulation tiles. The building dataset contains $1{,}310{,}254$ qualifying building polygons after applying the same $10\ \mathrm{m}^2$ minimum-area filter used for geometry generation, and the processed URAY tile set contains $7{,}657{,}880$ resolved tree crowns.

https://doi.org/10.5194/egusphere-2026-5226
Preprint. Discussion started: 9 September 2026

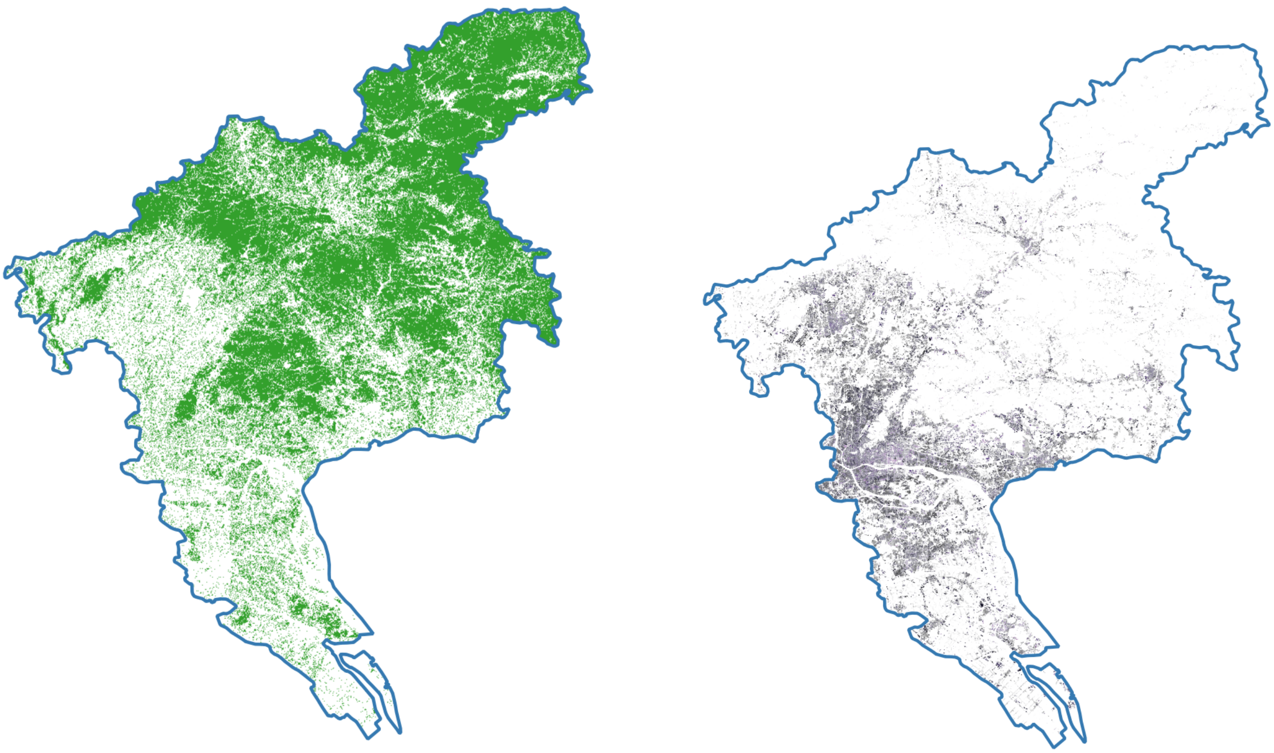

(a) Tree canopy height GIS layer

(b) Building footprint and height GIS layer

Figure 4. Full-city Guangzhou GIS inputs used to generate the URAY simulation tiles. Panel (a) shows the tree canopy height distribution derived from the very high resolution canopy height product of Tolan et al. (2024), and panel (b) shows the building footprint and building height data from 3D-GloBFP (Che et al., 2024). These layers are clipped to the same 1 km grid before each tile is converted into explicit three-dimensional building STL geometry and ellipsoidal tree crown inputs for the Monte Carlo albedo simulation.

First, the city-scale building and tree GIS layers are projected to a metric coordinate system and clipped to a common regular grid, with each cell assigned a unique tile identifier. Second, each valid tile is converted into model geometry: building footprints and heights are extruded into wall, roof, and ground STL surfaces, while the tree canopy height layer is segmented into individual crowns and exported as ellipsoidal tree parameters in a CSV file. Third, URAY runs the diurnal shortwave simulation for each tile using the matched STL, tree CSV, surface optical parameters, and hourly solar forcing. This step produces albedo and component absorption diagnostics for every daylight time step. Fourth, the tile outputs are joined back to the original GIS grid using the same tile identifier, allowing maps, city-scale statistics, and morphology-stratified comparisons to be generated from physically traceable simulation results.

The same tile identifier is preserved from the split GIS layers to the STL geometry, tree CSV, hourly output tables, and final albedo summary. This identifier makes each mapped simulation result traceable to its corresponding physical location and to the building and tree geometry used in the ray-tracing calculation.

https://doi.org/10.5194/egusphere-2026-5226
Preprint. Discussion started: 9 September 2026

The Guangzhou simulations were run for 29 January 2024 00:00 to 1 February 2024 23:00 local time (UTC+8) at hourly resolution, giving 96 time steps and 44 sunlit time steps for each tile. The city-scale run used 10^5 photons per time step and assigned the same baseline shortwave albedo of 0.28 to ground, wall, and roof surfaces. This value represents the high-solar-elevation, near-normal-incidence material albedo; for lower solar elevations, the model increases the effective material albedo using the Snell–Fresnel incidence-angle dependence, so the ray-tracing calculation accounts for solar-elevation effects through both hourly solar geometry and angle-dependent surface reflectance. The tree parameters used a uniform $\mathrm{LAD} = 3.0\ \mathrm{m}^2\,\mathrm{m}^{-3}$ and $G(\theta) = 1$, corresponding to the angle-independent projection assumption used in the baseline simulation. Across the 6761 completed simulation tiles, the generated urban geometry comprised $18{,}309{,}620$ surface elements in total. On a workstation equipped with an NVIDIA GeForce RTX 5090 D GPU, the batch runtime was 44,692.54 s, or 12.4 h in total, corresponding to an average of 465.55 s per hourly city-scale time step for all 6761 completed tiles.

3 Model validation

The validation is designed to test whether URAY can reproduce the main radiative processes required for coupled building and tree shortwave transfer: transmission and scattering within a tree crown, and three-dimensional radiation exchange in finite urban block geometry. No single experiment constrains both processes, so this study uses two complementary evaluation cases.

The first is the IsoTree benchmark of Bailey et al. (2014), which tests whether the canopy formulation can reproduce reflected shortwave fluxes above the canopy and transmitted photosynthetically active radiation within the canopy. The second is a SO-MUCH three-dimensional block experiment in Guangzhou, which tests whether the coupled model can reproduce albedo over a finite building array with trees. Together, these two benchmarks provide evidence that the model can represent canopy attenuation and scattering as well as three-dimensional building–tree radiation exchange before it is applied to city-scale Guangzhou simulations.

3.1 IsoTree canopy validation

The IsoTree experiment is used first to validate the tree transmissivity and scattering formulation in URAY. The experiment was conducted by Bailey et al. (2014) at the University of Utah campus. It measured the transmitted solar radiation within an isolated tree crown and the reflected shortwave radiation above the canopy. The IsoTree measurement geometry is plotted in Figure 5. In this experiment, an isolated Freeman maple with an approximately ellipsoidal crown was considered. Bailey et al. (2014) report that the crown was centered about 4.0 m above ground level and had a horizontal radius of 2.0 m and a vertical radius of 3.25 m. They also report a leaf area density of $0.8 \pm 0.7\ \mathrm{m}^{-1}$ from LAI2000 measurements. Following Bailey et al. (2014), the projection factor $G(\theta)$ was set to equal to 1.

The transmissivity of the tree crown was measured by two PAR sensors. PAR1 was installed just above the canopy along a pole aligned with the trunk, where it measured the incoming radiation incident on the crown. PAR2 was placed inside the crown, 1.8 m from the trunk, 85° clockwise from north, and 2.0 m above ground, where it measured the transmitted PAR after

https://doi.org/10.5194/egusphere-2026-5226
Preprint. Discussion started: 9 September 2026

radiation passed through the crown volume. The observed canopy transmissivity is therefore calculated from the ratio of PAR2 to PAR1.

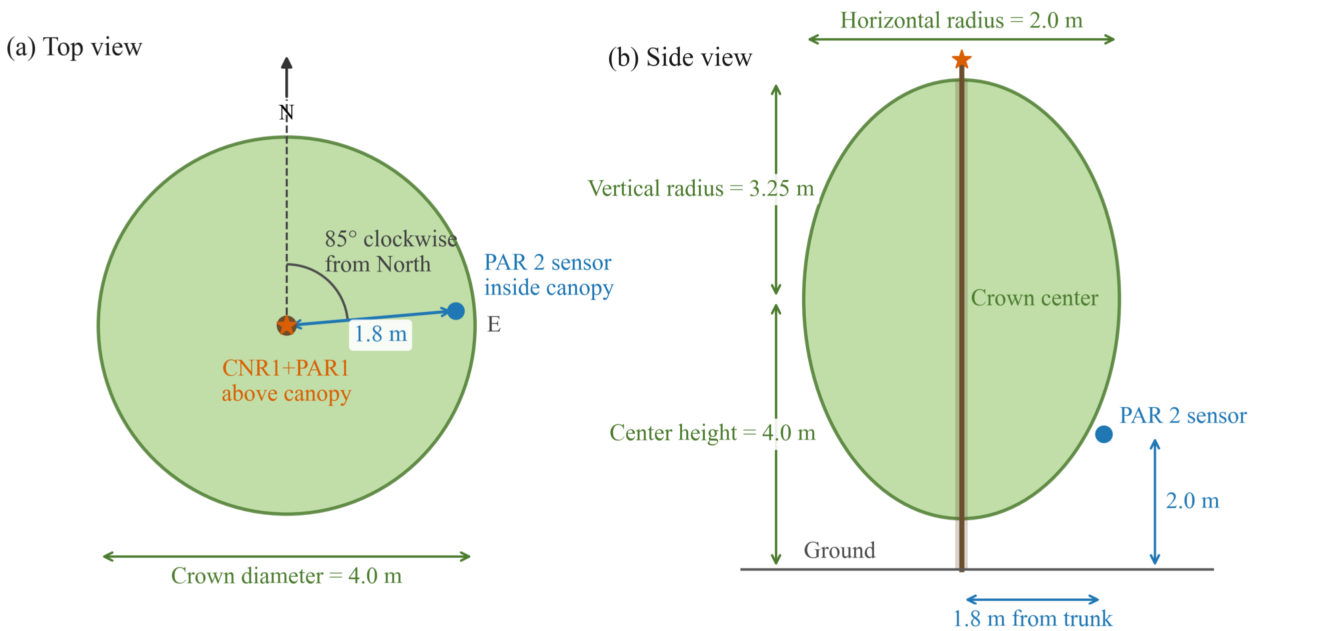

Figure 5. IsoTree benchmark geometry and sensor layout based on Bailey et al. (2014). The crown is represented as an ellipsoid with a horizontal radius of 2.0 m, a vertical radius of 3.25 m, and a center height of 4.0 m. The lower PAR sensor is located 1.8 m from the trunk, 85° clockwise from north in plan view, and 2.0 m above ground in side view, while the CNR1 radiometer and the upper PAR sensor are mounted above the canopy along the trunk axis.

In the IsoTree validation, URAY is evaluated by comparing the radiation at PAR2. The PAR1 measurement above the canopy is used as the incoming radiation input, while the single tree is represented in URAY as an ellipsoidal participating medium with the geometry described above. The model then predicts the transmitted PAR at the PAR2 location inside the crown. Figure 6 compares the measured and simulated PAR2 time series, showing that URAY captures the broad diurnal variation of under-canopy radiation. This validation demonstrates the capability of URAY to represent the time-varying transmittance of a complex three-dimensional tree crown.

https://doi.org/10.5194/egusphere-2026-5226
Preprint. Discussion started: 9 September 2026

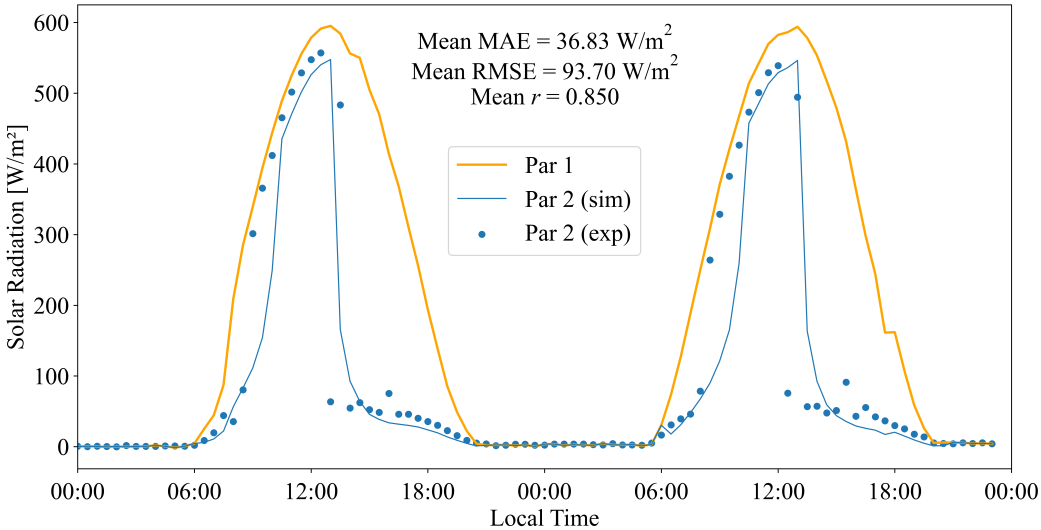

Figure 6. IsoTree validation for the canopy component of URAY. The figure compares incoming PAR1, simulated PAR2, and measured PAR2, with MAE, RMSE, and Pearson correlation coefficient r reported for the simulated and measured PAR2 comparison.

3.2 SOMUCH three-dimensional block albedo validation

The second validation uses a scaled outdoor experiment conducted at the SOMUCH (Scaled Outdoor Measurement of Urban Climate and Health) platform in Guangzhou. The experiment adopts a finite three-dimensional building layout rather than an idealized two-dimensional canyon section. This setting is used to test whether URAY can reproduce albedo over a block scale urban geometry with explicit buildings and tree crowns after the canopy transmissivity formulation has been tested with IsoTree. The paired treatments without and with vegetation provide a direct comparison of the same building arrangement under different canopy conditions. The validation focuses on the 2.0 m radiometer level, where the case without vegetation and the case with vegetation provide paired upward and downward shortwave measurements. Albedo is calculated as $K^{\uparrow}/K^{\downarrow}$ during daytime.

Figure 7 shows the experimental setup for the SOMUCH three-dimensional block validation, which was conducted in Guangzhou, China, from 29 October to 26 November 2023. The layout consists of a finite array of 12 building blocks arranged in three columns and four rows. The trees are represented by ellipsoidal crowns with a centre height of 0.55 m and a horizontal diameter of 0.5 m, arranged in three rows between the building columns. The CNR4 radiometer is mounted above the canopy at 2.0 m height and provides the upward and downward shortwave fluxes used for albedo calculation.

In URAY simulations of the SOMUCH validation, the same building and canopy geometry is reconstructed from the experimental layout, and the same shortwave forcing is applied. The canopy parameters are $\mathrm{LAD} = 3.5\ \mathrm{m^2\,m^{-3}}$ and $\chi = 1$. Ground,

https://doi.org/10.5194/egusphere-2026-5226
Preprint. Discussion started: 9 September 2026

wall, and roof albedos are all set to 0.24, and the canopy optical probabilities use the same baseline values as in the model description, $\omega_{LS} = 0.30$ and $\omega_{LD} = 0.80$.

The radiometer records total downward shortwave radiation $K^{\downarrow}$, but URAY requires separate direct and diffuse horizontal irradiance. For each time step, $K^{\downarrow}$ is treated as global horizontal irradiance, the solar zenith angle θ_z is calculated from the timestamp and the Guangzhou site coordinates, and the Boland diffuse-fraction model is used to estimate diffuse horizontal irradiance and direct normal irradiance. The direct and diffuse components are then used to launch the corresponding photon ensembles in URAY, and the simulated albedo is compared to the observed albedo at 2.0 m height for both the no-tree and tree cases.

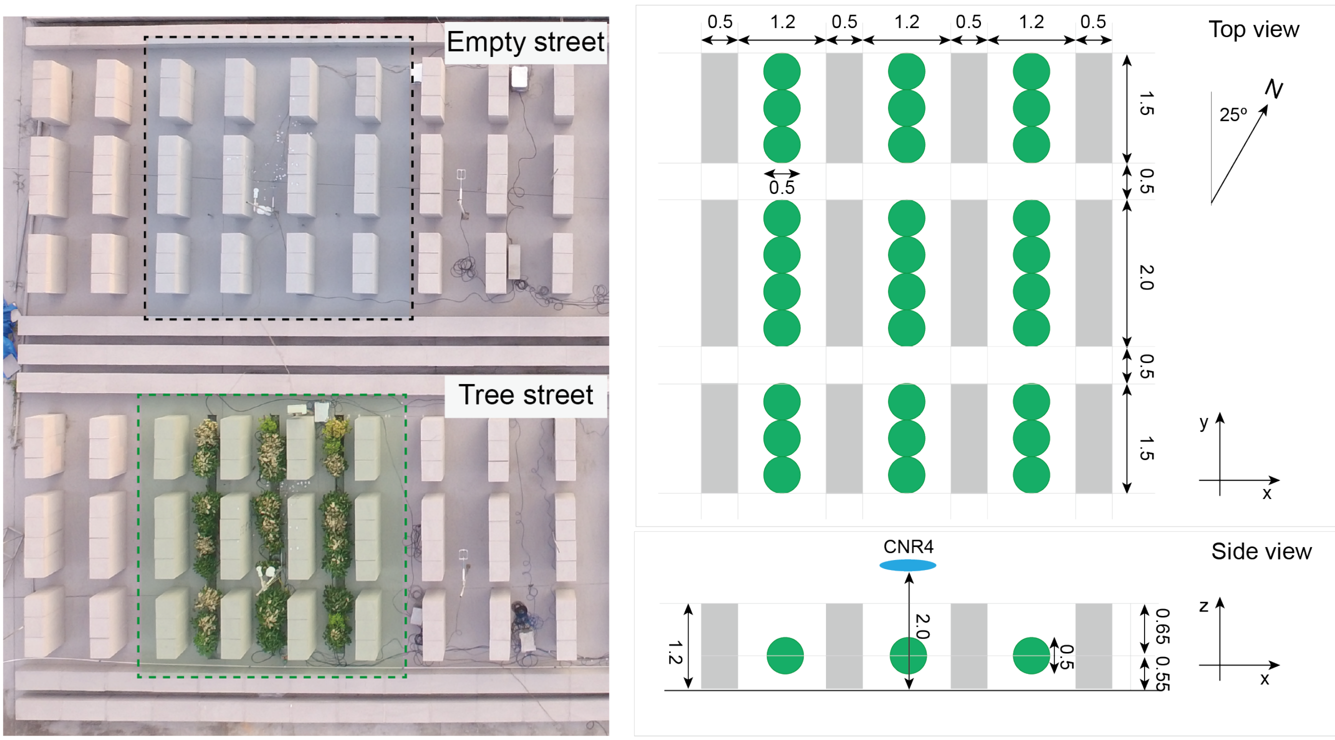

Figure 7. SOMUCH outdoor experimental setup used for the three-dimensional block albedo validation in Guangzhou. The figure shows the street layouts without and with trees, the corresponding plan view arrangement of buildings and tree crowns, and the side view CNR4 radiometer setup used to measure shortwave albedo.

Figure 8 compares SOMUCH measurements with URAY simulations for the full validation period, while Table 1 separates the statistics by solar elevation and surface-weather regime. Solar elevation was calculated from each 10 min timestamp and the site coordinates. The primary validation regime was defined as solar elevation $\geq 15°$, while records between $0°$ and $15°$ were reported separately as the low-sun regime. Rain-affected records were also separated based the observed rain days 29 October and 10–11 November 2023. Metrics were calculated from all paired records within each stratum rather than by averaging daily metrics; bias is defined as simulated minus observed albedo.

https://doi.org/10.5194/egusphere-2026-5226
Preprint. Discussion started: 9 September 2026

Under dry conditions with solar elevation $\geq 15°$, the empty-street case had MAE $= 0.0209$, RMSE $= 0.0244$, and bias $= -0.0004$, while the tree-street case had MAE $= 0.0172$, RMSE $= 0.0226$, and bias $= 0.0121$. These error statistics show that URAY reproduced the observed albedo magnitude closely under dry, high-sun conditions; the remaining temporal mismatches are visible in Fig. 8. During rain at the same solar-elevation threshold, MAE increased to 0.0495 for the empty street and 0.0381 for the tree street, with positive biases of 0.0472 and 0.0192, respectively, consistent with surface optical states that differ from the prescribed dry-material albedos. The low-sun dry regime produced RMSE values of 1.0348 and 0.6328 despite substantially smaller MAE values of 0.2300 and 0.1868 for the empty and tree streets, confirming that a small number of extreme ratio residuals dominate the unfiltered full-period RMSE. Because albedo is calculated as $K^{\uparrow}/K^{\downarrow}$, these records are especially sensitive to measurement noise, timing mismatch, and local shading when $K^{\downarrow}$ is small.

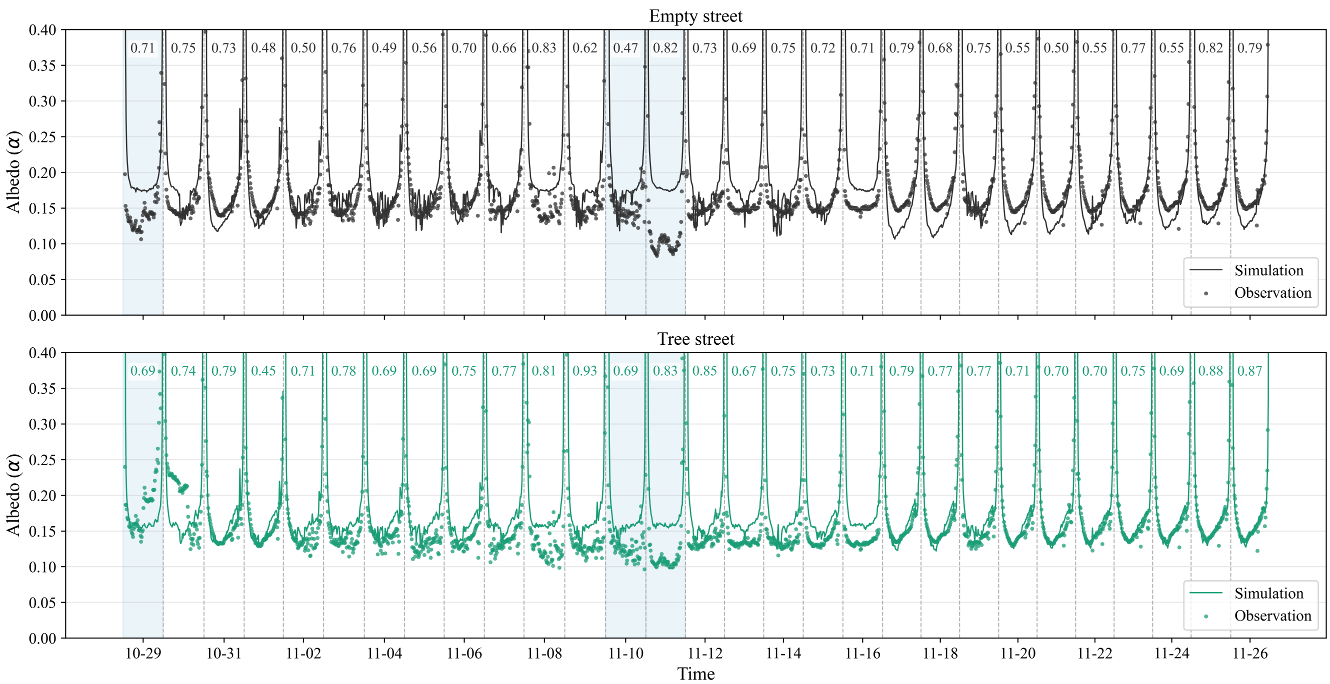

Figure 8. Continuous SOMUCH three-dimensional block albedo validation for 29 October–26 November 2023. The upper panel shows the street layout without trees and the lower panel shows the street layout with trees. Nighttime periods are omitted, vertical dashed lines separate consecutive days, the numbers above each day indicate the Pearson correlation coefficient r, and the blue shaded periods indicate rainy days. The comparison uses the 2.0 m measurement level and tests whether URAY reproduces observed albedo in a finite three-dimensional experimental layout. The 1–4 November 2023 records provide a representative daily sequence in which simulated and observed albedo are compared for the street layouts without and with trees, illustrating how the model reproduces the observed daytime albedo evolution and the difference between the two layout cases.

https://doi.org/10.5194/egusphere-2026-5226
Preprint. Discussion started: 9 September 2026

Table 1. SOMUCH albedo validation statistics stratified by solar elevation and weather regime. Metrics are pooled across paired 10 min records. Rain denotes 29 October and 10–11 November 2023; all other dates are classified as dry. Bias is simulated minus observed albedo.

Case	Solar elevation	Regime	N	MAE	RMSE	Bias
Empty street	$\geq 15°$	Dry	1341	0.0209	0.0244	-0.0004
Empty street	$\geq 15°$	Rain	155	0.0495	0.0559	0.0472
Empty street	0–15°	Dry	360	0.2300	1.0348	-0.0691
Empty street	0–15°	Rain	42	0.2102	0.5101	0.0061
Tree street	$\geq 15°$	Dry	1341	0.0172	0.0226	0.0121
Tree street	$\geq 15°$	Rain	155	0.0381	0.0436	0.0192
Tree street	0–15°	Dry	368	0.1868	0.6328	-0.0446
Tree street	0–15°	Rain	42	0.1758	0.3144	-0.0333

3.3 GPU acceleration, numerical convergence, and model sensitivity

This section first quantifies the computational advantage provided by GPU photon tracing. We used the representative Guangzhou tile shown in Figure 2 to compare a sequential CPU ray-tracing implementation with the GPU implementation under the same BVH-off setting. The benchmark was run on an Intel Core Ultra 9 285K CPU and an NVIDIA GeForce RTX 5090 D GPU. The selected benchmark time step was 1 February 2024 12:00 local time. The scene contained 767 resolved tree crowns and 18,656 surface elements, and the photon number was varied from 10^3 to 10^6 while keeping the geometry, tree optical parameters, surface albedos, solar direction, and direct and diffuse irradiance fixed. The CPU case traces photons sequentially and tests each ray directly against the surface elements. The GPU case uses the same BVH-off ray-tracing logic but evaluates photons in parallel.

Figure 9 shows that GPU parallelization becomes increasingly advantageous as the photon count grows. At 10^3 photons, GPU launch overhead made the GPU case slower than the sequential CPU case (5.46 versus 2.44 s). For 10^4, 10^5, and 10^6 photons, however, runtime decreased from 23.254, 222.023, and 2190.716 s on the CPU to 1.538, 2.254, and 11.042 s on the GPU, corresponding to speedups of 15.1, 98.5, and 198.4, respectively, calculated from the unrounded runtimes before BVH acceleration was introduced. Because Monte Carlo radiative transfer relies on large photon ensembles to obtain stable estimates, GPU parallelization is a necessary part of making this method computationally practical for city-scale simulations.

https://doi.org/10.5194/egusphere-2026-5226
Preprint. Discussion started: 9 September 2026

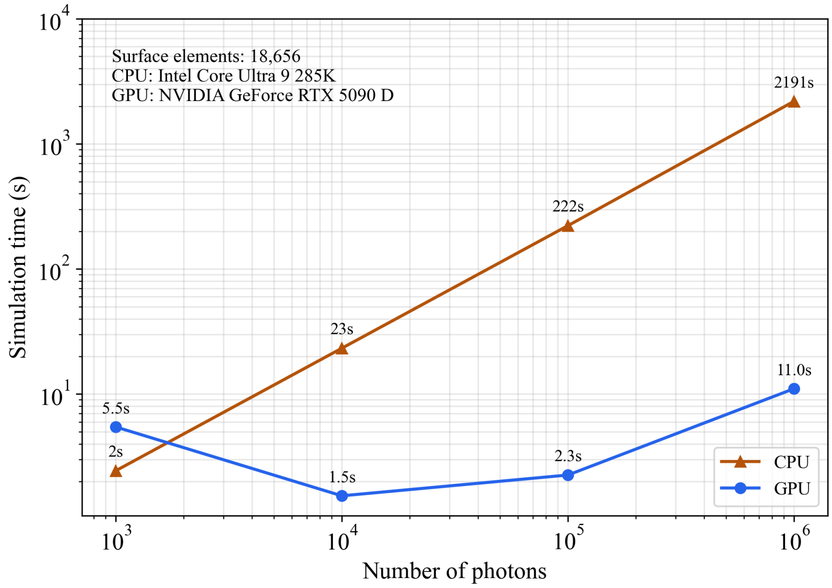

Figure 9. CPU and GPU runtime comparison for the BVH-off ray-tracing case in the representative Guangzhou tile. The benchmark uses the maximum-irradiance sunlit time step, 18 656 surface elements, and photon counts from 10^3 to 10^6. Both cases disable BVH acceleration; the CPU case traces photons sequentially, while the GPU case traces photons in parallel. GPU launch overhead dominates at 10^3 photons, whereas the GPU implementation is 15.1–198.4 times faster than the sequential CPU implementation for 10^4–10^6 photons.

A second performance test evaluated whether BVH acceleration changes the radiative solution or only the cost of ray–building intersection. The test used the same representative tile, geometry, radiative parameters, and 96 h forcing period, and increased the photon number to 10^6 per time step to reduce Monte Carlo noise when comparing acceleration settings. The scene contained 18 656 triangular urban surfaces. We compared a BVH-off reference with BVH-enabled simulations using maximum leaf sizes of 1, 2, 4, 8, 16, 32, and 64. The maximum leaf size is stored in a terminal BVH node before traversal switches from hierarchy traversal to direct triangle-intersection tests. Smaller leaf sizes create deeper hierarchies with fewer primitives per leaf, whereas larger leaf sizes reduce hierarchy depth but require more direct intersection tests in each terminal node. As shown in Figure 10, enabling BVH changed daylight mean albedo and ground absorption by only 10^{-5}–10^{-6} relative to the BVH-off reference. In contrast, BVH acceleration reduced the wall-clock time for the full 96 h test from 650.6 s to 48.8–60.6 s. The weak dependence of the radiative diagnostics on maximum leaf size indicates that the BVH setting primarily controls computational efficiency, not the interpreted radiation budget. This measured acceleration is a conservative implementation result rather than an algorithmic upper limit, because further improvements in BVH construction, node layout, traversal order, and GPU memory access could increase the speedup.

https://doi.org/10.5194/egusphere-2026-5226
Preprint. Discussion started: 9 September 2026

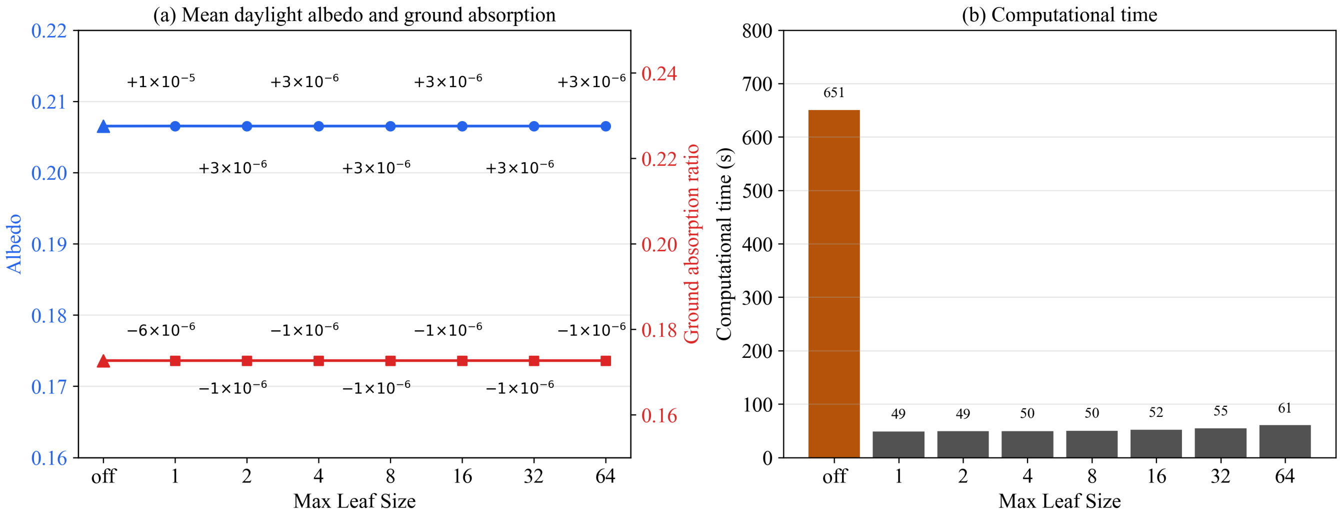

Figure 10. BVH acceleration sensitivity test for the representative Guangzhou tile shown in Figure 2. Panel (a) compares daylight mean scene albedo and ground absorption ratio using a double y axis; formula labels show the differences between each BVH-enabled simulation and the BVH-off reference. Panel (b) shows the corresponding wall-clock time for the full 96 h simulation. Maximum leaf size denotes the upper limit on the number of triangular building primitives stored in a terminal BVH node.

The GPU and BVH benchmarks establish the computational basis for applying URAY to city-scale Guangzhou tiles, but the radiative diagnostics must also be checked for numerical and physical sensitivity. The numerical sensitivity comes from the Monte Carlo solver: too few photons would make albedo and absorption diagnostics fluctuate because of sampling noise rather than because of geometry or tree effects. Photon number is therefore tested to identify a practical ensemble size for large batches while confirming that the interpreted signals are not dominated by random sampling error. The physical sensitivity comes from canopy structure: canopy attenuation is controlled mainly by crown path length, LAD, and the leaf angle parameter χ, but LAD and χ are effective structural parameters in the city-scale workflow rather than directly measured for every tree. Sensitivity tests for LAD and χ are therefore used to quantify how uncertainty in canopy structure propagates into scene albedo and ground absorption.

The photon number test was conducted with the representative Guangzhou tile shown in Figure 2. The same building geometry, tree crown parameter, radiative parameters, weather forcing, BVH settings, and time window were held fixed for all cases. Only n_{photons} was varied, using eight logarithmically spaced values: 10,000, 26,827, 71,969, 193,070, 517,947, 1,389,495, 3,727,594, and 10,000,000 photons per time step. For each photon count, the simulation ran the full hourly sequence from 29 January 2024 00:00 to 1 February 2024 23:00 local time, giving 96 hourly records and 44 daylight time steps.

Figure 11 compares the hourly albedo and ground absorption ratio for all photon counts, while the daylight mean diagnostics are summarized in panels (c) and (d). The hourly records show that the 10^4 photon case differs slightly from the 10^7 photon reference, while the 10^5 photon case is visually indistinguishable from the reference. The simulation also runs efficiently for

https://doi.org/10.5194/egusphere-2026-5226
Preprint. Discussion started: 9 September 2026

this complex urban tile. The two largest photon cases required 4.18 s per time step for 3.73×10^6 photons and 9.80 s per time step for 10^7 photons.

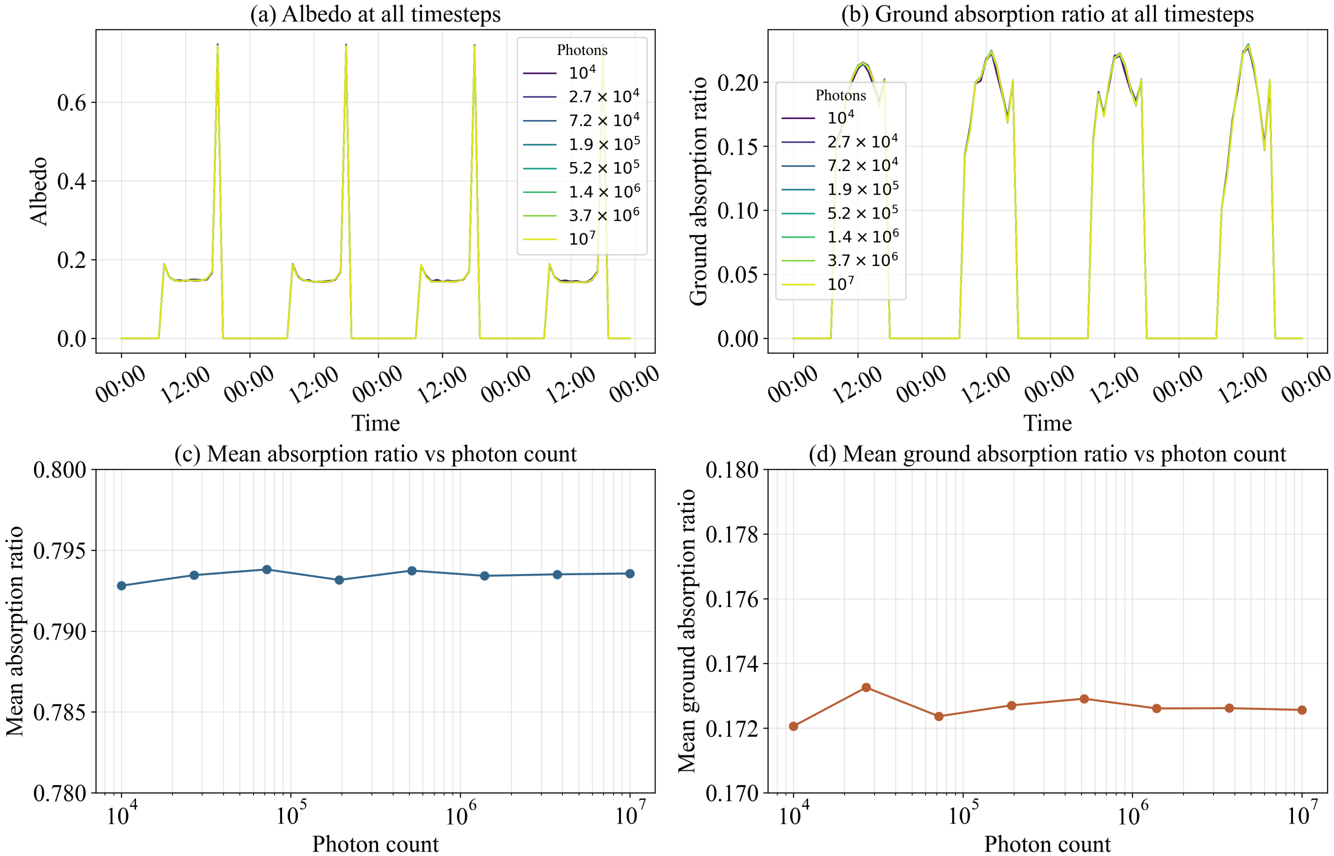

Figure 11. Photon number sensitivity test for the representative Guangzhou tile shown in Figure 2, which contains both buildings and tree crowns. Panels (a) and (b) compare hourly scene albedo and ground absorption ratio for all photon counts. Panels (c) and (d) summarize daylight mean total absorption and ground absorption as functions of photon count. The weak dependence of the mean diagnostics above the operational 10^5 photon scale indicates that the city-scale batch setting is not dominated by Monte Carlo sampling noise.

The daytime mean diagnostics exhibit clear convergence at 10^5 photons. Relative to the 10^7 photon reference, the 10^4 photon case differs by 7.5×10^{-4} in mean albedo and 5.0×10^{-4} in mean ground absorption. For photon counts near the operational 10^5 scale, the differences remain on the order of 10^{-4}. This level of variation is small compared with the expected spatial contrasts between scenes with and without trees in city-scale applications, indicating that $n_{\text{photons}} = 100{,}000$ per time step is an appropriate computational compromise for large batches.

Together, the photon-count analysis and acceleration benchmarks separate numerical sampling and computational settings from the remaining physical assumptions. Two additional sensitivity tests for canopy structure were conducted for LAD and $G(\theta)$, because these parameters were treated as assumptions in the validation cases. The purpose of these tests is to evaluate

https://doi.org/10.5194/egusphere-2026-5226
Preprint. Discussion started: 9 September 2026

how much the assumed canopy density and leaf projection behaviour can influence the radiation budget when the model is applied to a real urban configuration with dense tree and building cover. Since LAD and $G(\theta)$ enter the crown extinction coefficient through $\sigma_t = \mathrm{LAD}\, G(\theta)$, their values can alter photon interception, canopy absorption and transmission, ground absorption, and the resulting scene albedo at tile scale. The tests used the same representative tile, geometry, forcing period, surface albedos, optical probabilities, and operational photon number of $n_{\mathrm{photons}} = 100{,}000$ per time step.

First, LAD was multiplied by a perturbation factor,

$$\mathrm{LAD}' = f_{\mathrm{LAD}} \mathrm{LAD}_0,$$

while crown geometry, tree location, χ, canopy optical probabilities, surface albedos, forcing, and photon number were held fixed. Eight LAD cases were evaluated: $f_{\mathrm{LAD}} = 0.25, 0.5, 0.75, 1.0, 1.25, 1.5, 1.75$, and 2.0. This factor range spans from very open to dense crowns around the baseline derived from GIS data without changing the crown volume itself. For Guangzhou, the factors are applied to each tile's own baseline LAD so that spatial differences in crown density are preserved.

Second, the assumption $G(\theta) = 1$ is tested. The projection function is (Campbell, 1986)

$$G(\theta) = \frac{\chi}{\sqrt{\chi^2 \cos^2\theta + \sin^2\theta}}.$$

During the simulation, we assume $G(\theta) = 1$ for all incident directions, so the canopy extinction becomes $\sigma_t = \mathrm{LAD}$ and angular effects of leaf projection are suppressed. Eight χ cases were evaluated: $\chi = 0.25, 0.5, 0.75, 1.0, 1.25, 1.5, 2.0$, and 4.0. The central range $\chi = 0.5$–2.0 represents leaf-angle structures ranging from more horizontal to more vertical, while $\chi = 0.25$ and 4.0 are retained as wider structural stress tests. Across solar zenith angles this range brackets substantially different $G(\theta)$ responses, with $\chi = 1$ as the angle independent baseline. The LAD and χ tests are evaluated with the same daylight mean diagnostics as the photon number test, including scene albedo, ground absorption ratio, wall and roof absorption, canopy absorption, and tile level differences relative to the baseline case.

https://doi.org/10.5194/egusphere-2026-5226
Preprint. Discussion started: 9 September 2026

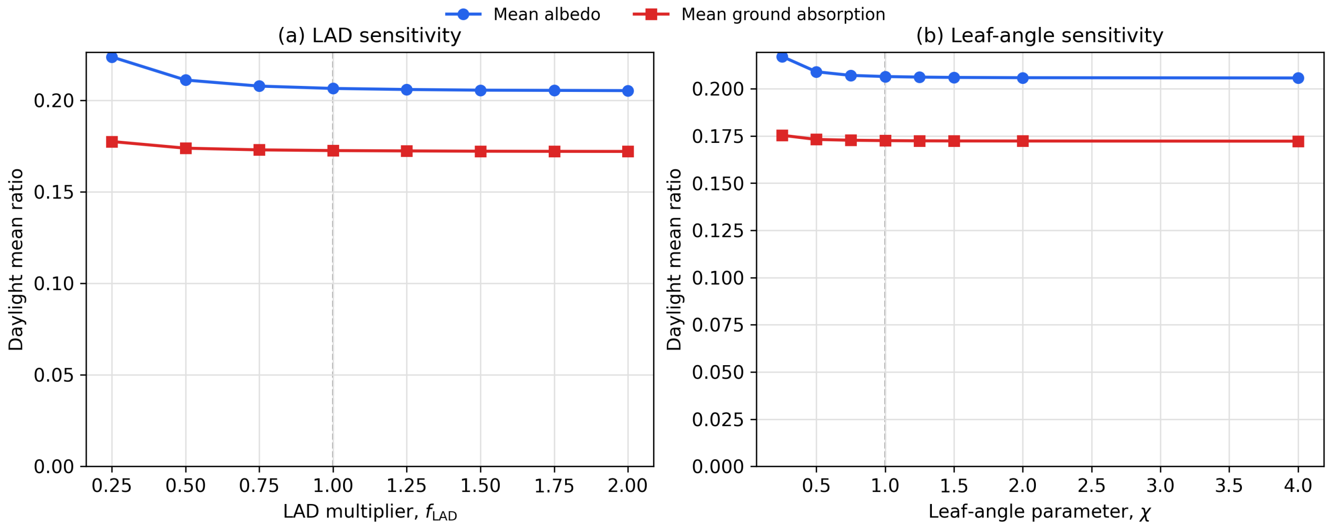

Figure 12. Sensitivity test for canopy structure in the representative Guangzhou tile shown in Figure 2 using 10^5 photons per time step. Panel (a) shows the sensitivity to the LAD multiplier f_{LAD}, and panel (b) shows the sensitivity to the leaf angle parameter χ.

The results show that both diagnostics are most sensitive when the canopy is made substantially more open than the baseline. Reducing LAD to $0.25\mathrm{LAD}_0$ increases daylight mean albedo from 0.2064 to 0.2237 and increases mean ground absorption from 0.1725 to 0.1774, whereas increasing LAD beyond the baseline produces a weaker and saturating response, with albedo decreasing to 0.2053 and ground absorption to 0.1720 at $2.0\mathrm{LAD}_0$. The χ perturbation shows a similar but smaller monotonic effect: changing χ from 0.25 to 4.0 decreases albedo from 0.2171 to 0.2057 and decreases ground absorption from 0.1753 to 0.1722. Thus, for this dense tile with trees, the current $\chi = 1$ assumption is not the dominant source of variation relative to large LAD reductions, but canopies with low χ still modify the tile scale radiation budget enough to justify retaining χ as an explicit sensitivity parameter.

4 City-scale shortwave redistribution in Guangzhou

The Guangzhou experiment tests whether explicit building–tree shortwave radiative transfer can be used as a city-scale diagnostic. Using the workflow described in Section 2.5, URAY was run over Guangzhou from 29 January 2024 00:00 to 1 February 2024 23:00 local time at hourly resolution. The batch simulation used 10^5 photons per time step and processed 6761 valid 1 km tiles on an NVIDIA GeForce RTX 5090 D GPU, with a total runtime of 44,692.54 s and an average of 465.55 s per hourly city-scale time step.

Figure 13 shows the simulated albedo and ground absorption ratio across Guangzhou. Because the simulations span multiple days, both metrics were first averaged over daytime hours for each day and then used to map their spatial patterns. The results reveal strong spatial heterogeneity in both albedo and ground absorption ratio. In mesoscale models, the surface energy balance is usually represented mainly through albedo, but this treatment can overlook the redirection of solar energy by urban geometry.

https://doi.org/10.5194/egusphere-2026-5226
Preprint. Discussion started: 9 September 2026

By resolving three-dimensional urban geometry, URAY not only estimates surface albedo but also reveals how solar energy is redistributed within urban areas. Compared with albedo, the ground absorption ratio more directly represents how much solar energy is absorbed by ground surfaces, and therefore may better indicate processes related to near-surface air temperature, heat storage, shading effects, and urban heat exposure.

Overall, the albedo and ground absorption ratio maps show similar spatial patterns, with areas of low albedo generally corresponding to low ground absorption ratio. Notably, these low-value areas are mainly found in forested regions rather than built-up areas. This indicates that, in Guangzhou's urban environment, low albedo does not necessarily imply stronger ground-level solar absorption; vegetation cover and shading effects also strongly influence the amount of solar radiation received and absorbed by ground surfaces.

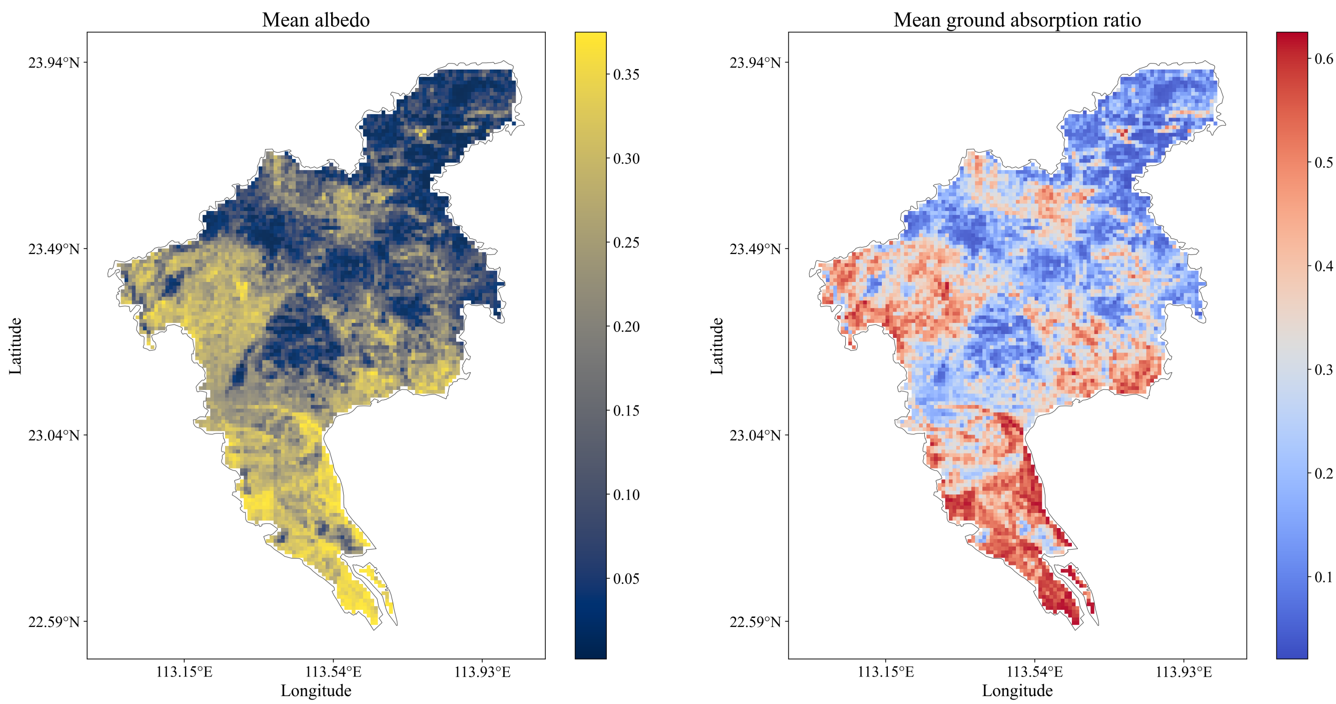

Figure 13. City-scale simulation results generated by URAY. Each polygon is a 1 km grid tile of Guangzhou. Panel (a) maps the mean daytime scene albedo of each tile over 29 January–1 February 2024. Panel (b) maps the corresponding daytime mean fraction of incident shortwave radiation absorbed by the ground surface. Panel (c) maps the daytime mean wall absorption ratio, and panel (d) maps the daytime mean roof absorption ratio. Scene albedo can exceed the 0.28 reference material albedo because surface reflectance is incidence-angle corrected and α is a scene-level escape fraction.

To further examine the relationship between ground shortwave absorption and albedo, we performed a regression analysis between mean daytime albedo and mean daytime ground absorption ratio across the 6,761 completed simulation tiles in Guangzhou. The two diagnostics are strongly and nearly linearly correlated ($r = 0.942$, $R^2 = 0.888$), with a fitted linear relationship of $A_g = 1.377\alpha + 0.054$, where A_g is the mean ground absorption ratio and α is the mean scene albedo. This

https://doi.org/10.5194/egusphere-2026-5226
Preprint. Discussion started: 9 September 2026

relationship does not imply that higher albedo causes greater ground shortwave absorption. Instead, the regression indicates that albedo and ground absorption ratio are shaped by shared spatial controls, including urban form, land cover, and shading conditions. High albedo and high ground absorption tend to occur together in open or weakly vegetated tiles, where shortwave radiation can both reach the ground and escape upward after reflection. As a check against daylight averaging, the same relationship was evaluated at 13:00 local time on 29 January 2024 and remained strong ($A_g = 2.018\alpha + 0.062$, $r = 0.959$, $R^2 = 0.920$; Appendix A).

We further stratified the regression analysis by urban morphology to test whether the city-wide albedo–ground absorption relationship changes with building density and tree density. Tiles were divided into four classes using median splits of building surface count and tree count: high and low building density were defined relative to the median building surface count, and high and low tree density were defined relative to the median tree count.

The morphology-stratified results in Figure 14 show that the positive albedo–ground absorption relationship persists within each morphology class, but its slope, scatter, and occupied range vary with building and tree density. Within the high-building-density class, the relationship is stronger for tiles with high tree density ($r = 0.914$) than for those with low tree density ($r = 0.733$). Thus, abundant trees strengthen the relationship within densely built tiles while shifting its occupied albedo and ground-absorption ranges. Trees and buildings affect shortwave redistribution through different mechanisms. For trees, the canopy intercepts, absorbs, and scatters incoming shortwave radiation; as tree density increases, more energy is absorbed by the canopy, and less shortwave radiation reaches the ground. For buildings, consistent with the three-dimensional morphology controls described by Mei et al. (2025), deep canyons in high-density areas promote multiple reflections and trap more shortwave radiation. At the same time, a higher roof-area fraction can increase the amount of reflected shortwave radiation escaping upward. Thus, the effect of building density on albedo and ground absorption ratio is not unidirectional, but depends on the combined effects of canyon trapping, roof reflection, and ground shading.

Urban albedo is widely used as an indicator of urban heat exposure and surface energy balance, with lower albedo generally associated with greater heat absorption and stronger urban heat island effects. However, the Guangzhou results show that low albedo does not necessarily correspond to high ground absorption, which is more directly linked to pedestrian heat exposure. In dense built-up areas with abundant trees, this relationship becomes more complex, highlighting the need to explicitly resolve shortwave absorption redistribution in complex three-dimensional urban geometry.

https://doi.org/10.5194/egusphere-2026-5226
Preprint. Discussion started: 9 September 2026

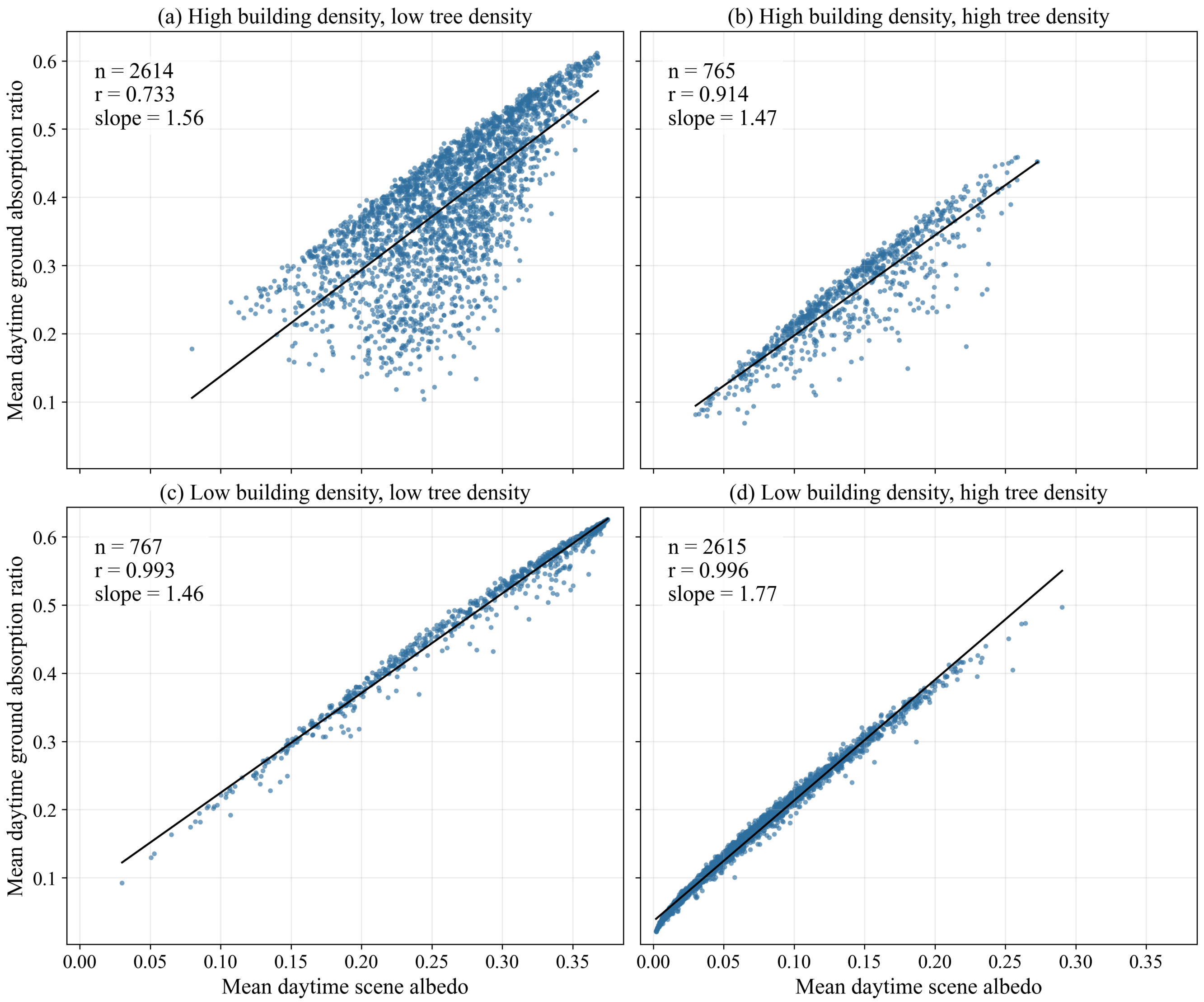

Figure 14. Morphology-stratified relationship between daytime mean scene albedo and daytime mean ground absorption ratio for the 6,761 completed Guangzhou simulation tiles. Tiles are divided into four classes using median splits of building surface count and tree count: high and low building density are defined relative to the median building surface count of 945, and high and low tree density are defined relative to the median tree count of 1071. Each panel shows one morphology class, with points representing 1 km simulation tiles. The black line shows the least-squares linear fit; panel annotations report sample size, Pearson correlation coefficient, and fitted slope. The stratification shows that the positive albedo–ground absorption relationship persists within morphology classes, while dense buildings and abundant trees shift the range and slope of the relationship.

https://doi.org/10.5194/egusphere-2026-5226
Preprint. Discussion started: 9 September 2026

5 Discussion

The Guangzhou city-scale simulation was designed as a showcase to test the feasibility of applying URAY to building- and tree-resolving shortwave radiative transfer across an entire city. Accordingly, several limitations define the scope of the current implementation and the interpretation of its results. First, tree-crown optical properties are represented using a simplified parameterization. The PROSPECT-based mapping uses a generic green broadleaf optical state rather than species-specific measurements for Guangzhou trees, and it averages $\rho(\lambda) + \tau(\lambda)$ over 400–2500 nm without resolving leaf age, water stress, seasonal pigment change, or solar-spectrum weighting. The parameter ω_{LS}, which partitions specular and diffuse scattering in the Monte Carlo kernel, is not directly returned by PROSPECT and therefore introduces additional uncertainty. These optical assumptions affect the balance among canopy absorption, upward scattering, and radiation transmitted to ground and walls.

Second, the Guangzhou simulation assigns a uniform baseline albedo to ground, walls, and roofs. This choice isolates building–tree radiative interactions but does not represent spatial variations in material type, ageing, colour, coating, or moisture state. The SOMUCH validation shows that wet urban surfaces can alter albedo, making rainfall and wet-surface optical properties important sources of uncertainty. The resulting city-scale maps should therefore be interpreted as scenario diagnostics conditioned on the prescribed surface properties rather than as a definitive reconstruction of Guangzhou's radiative state.

Third, GIS-derived tree crowns are reconstructed with a segmentation and ellipsoid-fitting algorithm that does not fully represent crown-shape complexity, species differences, branch structure, or within-crown heterogeneity. The IsoTree and SOMUCH experiments evaluate crown attenuation and block-scale albedo, respectively, but they do not independently validate city-wide component absorption under heterogeneous real-world conditions. In addition, URAY currently resolves shortwave radiation only; it does not simulate longwave exchange, the complete surface energy balance, air temperature, or thermal comfort. Consequently, the present results cannot be interpreted directly as estimates of cooling or planning benefits.

Despite these limitations, three conclusions remain useful within clearly defined boundaries. First, the validation and performance experiments support the methodological conclusion that explicit building surfaces and transmissive tree crowns can be coupled within a three-dimensional Monte Carlo framework and evaluated at city scale. BVH-accelerated intersections and GPU-parallel photon tracing preserve component-level radiative diagnostics while making simulations over thousands of urban tiles computationally practical. This conclusion concerns model architecture and computational feasibility and does not depend on treating the Guangzhou optical inputs as exact observations.

Second, the Guangzhou application supports a diagnostic conclusion: scene albedo alone does not identify where non-reflected shortwave energy is absorbed. Across the completed simulation tiles, scene albedo and ground absorption were positively correlated ($r = 0.942$) because open, sparsely treed areas allowed more sunlight to reach the ground and more reflected radiation to escape upward.

Third, the morphology-stratified analysis provides a useful hypothesis about the role of trees in dense urban settings. Within high-building-density areas, the albedo–ground absorption correlation increased from $r = 0.733$ under low tree density to $r = 0.914$ under high tree density. This contrast shows that the relationship between reflected and ground-absorbed shortwave

https://doi.org/10.5194/egusphere-2026-5226
Preprint. Discussion started: 9 September 2026

radiation varies systematically with tree density. URAY can therefore identify morphology-dependent radiative patterns and guide future paired simulations or field measurements designed to test their mechanisms.

Future development should combine higher-resolution crown geometry from drone LiDAR or comparable observations with mapped urban materials, moisture-dependent surface properties, species-specific optical measurements, and uncertainty propagation across geometric and optical inputs. Within its current scope, URAY is most useful as a physically explicit framework for analysing shortwave redistribution, testing hypotheses, and identifying where additional observations are needed.

6 Conclusions

URAY is a city-scale three-dimensional Monte Carlo model that resolves both buildings and trees for urban shortwave radiative transfer. It represents buildings as explicit triangulated surfaces and tree crowns as participating media, combined with Woodcock tracking and BVH acceleration on a GPU, so that scene albedo and absorbed shortwave radiation are diagnosed per surface component without relying on idealized two-dimensional canyon assumptions. The model was evaluated against two benchmark cases and then applied to a city-scale simulation. The IsoTree validation demonstrates that URAY captures canopy attenuation and scattering behaviour, while the SOMUCH case shows that the model reproduces realistic shortwave response in a three-dimensional urban block with trees.

The Guangzhou implementation demonstrates shortwave radiation analysis with explicit three-dimensional building and canopy geometry at city scale. In the city-scale simulation, URAY processed 6761 completed $1\ \mathrm{km}^2$ tiles containing approximately 1.3×10^6 building polygons, 7.7×10^6 resolved tree crowns, and 18×10^6 surface elements. A complete hourly city-scale time step required approximately 465.55 s on a consumer-class GPU. In the performance benchmarks, GPU parallelization was approximately 198 times faster than sequential CPU computation at 10^6 photons, while BVH acceleration reduced wall-clock time by approximately one order of magnitude. Together, these acceleration strategies make city-scale three-dimensional Monte Carlo radiative-transfer simulations computationally practical.

The Guangzhou application reveals how urban morphology and tree cover shape shortwave redistribution. Across the city, scene albedo and ground absorption were positively correlated ($r = 0.942$) because open, sparsely treed areas both exposed more ground to sunlight and allowed more reflected radiation to escape upward. Within high-building-density areas, this correlation increased from $r = 0.733$ under low tree density to $r = 0.914$ under high tree density, highlighting the role of canopy interception in regulating shortwave redistribution. These results demonstrate the importance of explicit three-dimensional geometry in accurately modeling urban shortwave radiation.

Appendix A: Instantaneous Guangzhou diagnostics at 13:00 local time

Figure A1 shows the instantaneous Guangzhou scene albedo and ground absorption ratio at 13:00 local time on 29 January 2024. The corresponding tile-scale relationship between instantaneous albedo and ground absorption ratio is shown in Figure A2.

https://doi.org/10.5194/egusphere-2026-5226
Preprint. Discussion started: 9 September 2026

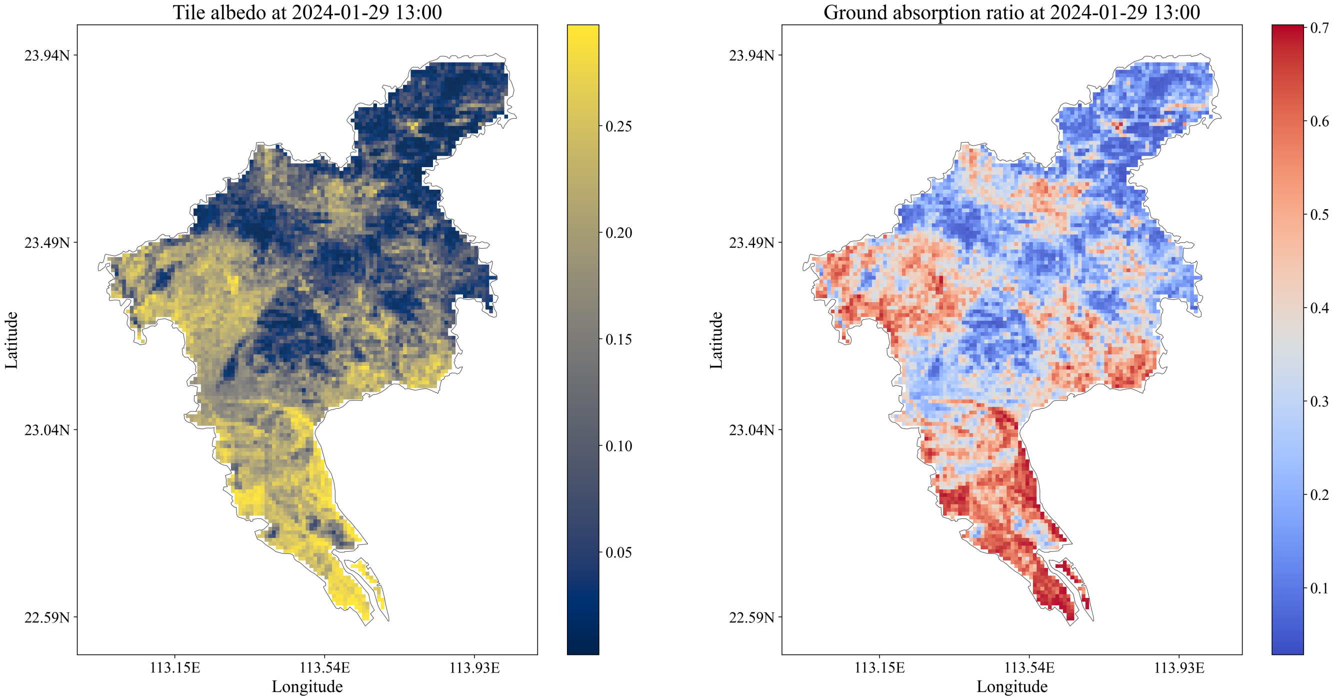

Figure A1. Instantaneous city-scale URAY diagnostics at 13:00 local time on 29 January 2024. Panel (a) maps scene albedo, and panel (b) maps the corresponding fraction of incident shortwave radiation absorbed by the ground surface.

https://doi.org/10.5194/egusphere-2026-5226
Preprint. Discussion started: 9 September 2026

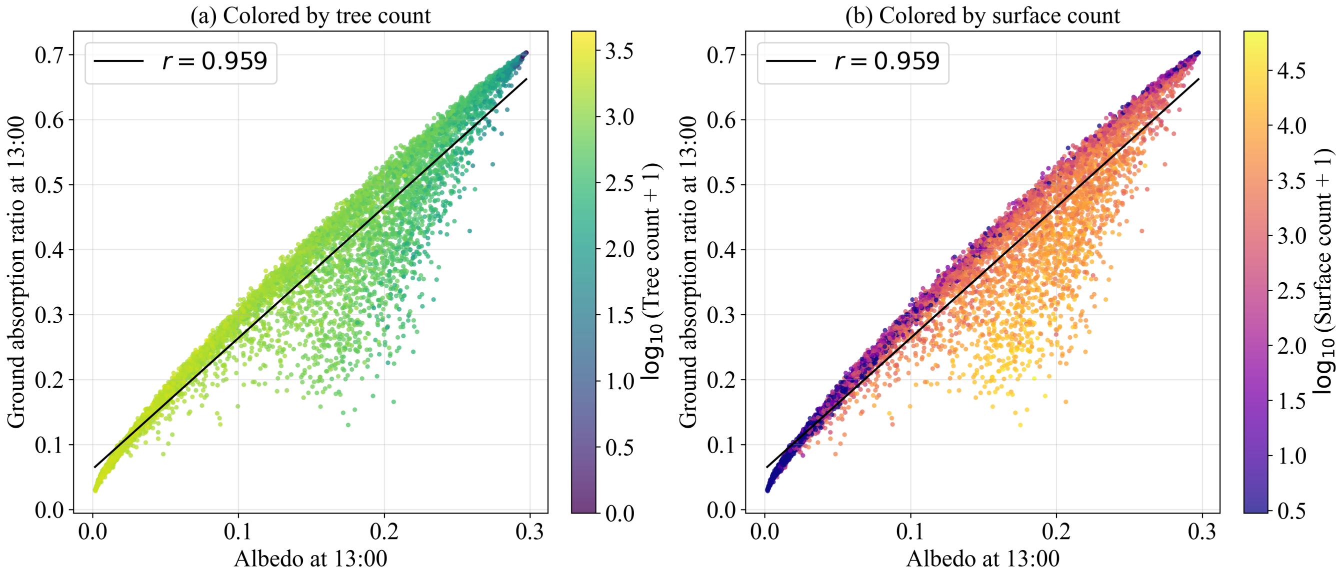

Figure A2. Relationship between instantaneous scene albedo and instantaneous ground absorption ratio at 13:00 local time on 29 January 2024 for the 6761 completed Guangzhou simulation tiles. Panel (a) colours each tile by $\log_{10}$ transformed tree count, and panel (b) colours each tile by $\log_{10}$ transformed building surface count. The black line shows the least-squares linear fit, with the Pearson correlation coefficient reported in each panel.

Code availability. The URAY source code is available from https://github.com/sj-mei/PyUray and is released under the MIT License. Version 1.0 is permanently archived on Zenodo at https://doi.org/10.5281/zenodo.22153465 (Mei and Sun, 2026).

Data availability. The validation and preprocessing assets used in this manuscript are included in the Zenodo archive at https://doi.org/10.5281/zenodo.22153465 (Mei and Sun, 2026). External geospatial input products are cited and linked according to their original data licences in the final submission.

Author contributions. SJM: conceptualization, methodology, software, formal analysis, and writing – original draft. ZW: investigation, validation, and writing – review and editing. JTH: investigation, validation, and writing – review and editing. TC: validation, resources, and writing – review and editing. GC: investigation, data curation, and writing – review and editing. TS: conceptualization and writing – review and editing.

https://doi.org/10.5194/egusphere-2026-5226
Preprint. Discussion started: 9 September 2026

Competing interests. At least one of the (co-)authors is a member of the editorial board of *Geoscienti ic Model Development*.

Acknowledgements. This research was supported by the National Natural Science Foundation of China (grant nos. 42305076, W2421048, and U2442212), the Natural Science Foundation of Guangdong Province (grant no. 2024A1515010173), the Organization Department of the Central Committee of the Communist Party of China (grant no. BH2023009), and the Royal Society (grant no. IEC\NSFC\242040). The authors acknowledge the repository development, validation assets, and urban-radiation experiment materials that support the URAY workflows summarized in the manuscript.

https://doi.org/10.5194/egusphere-2026-5226
Preprint. Discussion started: 9 September 2026

References

Akbari, H., Menon, S., and Rosenfeld, A.: Global cooling: increasing world-wide urban albedos to offset CO2, Climatic Change, 94, 275–286, https://doi.org/10.1007/s10584-008-9515-9, 2009.

Aida, M. and Gotoh, K.: Urban albedo as a function of the urban structure – A two-dimensional numerical simulation, Boundary-Layer Meteorology, 23, 415–424, https://doi.org/10.1007/BF00116270, 1982.

Arnfield, A. J.: An approach to the estimation of the surface radiative properties and radiation budgets of cities, Physical Geography, 3, 97–122, https://doi.org/10.1080/02723646.1982.10642221, 1982.

Arnfield, A. J.: Validation of an estimation model for urban surface albedo, Physical Geography, 9, 361–372, https://doi.org/10.1080/02723646.1988.10642360, 1988.

Bailey, B. N., Overby, M., Willemsen, P., Pardyjak, E. R., Mahaffee, W. F., and Stoll, R.: A scalable plant-resolving radiative transfer model based on optimized GPU ray tracing, Agricultural and Forest Meteorology, 198–199, 192–208, https://doi.org/10.1016/j.agrformet.2014.08.012, 2014.

Campbell, G. S.: Extinction coefficients for radiation in plant canopies calculated using an ellipsoidal inclination angle distribution, Agricultural and Forest Meteorology, 36, 317–321, https://doi.org/10.1016/0168-1923(86)90010-9, 1986.

Caliot, C., d'Alencon, L., Blanco, S., Forest, V., Fournier, R., Hourdin, F., Retailleau, F., Schoetter, R., and Villefranque, N.: Coupled heat transfers resolution by Monte Carlo in urban geometry including direct and diffuse solar irradiations, International Journal of Heat and Mass Transfer, 222, 125139, https://doi.org/10.1016/j.ijheatmasstransfer.2023.125139, 2024.

Fortuniak, K.: Numerical estimation of the effective albedo of an urban canyon, Theoretical and Applied Climatology, 91, 245–258, https://doi.org/10.1007/s00704-007-0312-6, 2008.

Che, Y., Li, X., Liu, X., Wang, Y., Liao, W., Zheng, X., Zhang, X., Xu, X., Shi, Q., Zhu, J., Zhang, H., Yuan, H., and Dai, Y.: 3D-GloBFP: the first global three-dimensional building footprint dataset, Earth System Science Data, 16, 5357–5374, https://doi.org/10.5194/essd-16-5357-2024, 2024.

Holmgren, W. F., Hansen, C. W., and Mikofski, M. A.: pvlib Python: a Python package for modeling solar energy systems, Journal of Open Source Software, 3, 884, https://doi.org/10.21105/joss.00884, 2018.

Jacquemoud, S. and Baret, F.: PROSPECT: A model of leaf optical properties spectra, Remote Sensing of Environment, 34, 75–91, https://doi.org/10.1016/0034-4257(90)90100-Z, 1990.

Feret, J.-B., Gitelson, A. A., Noble, S. D., and Jacquemoud, S.: PROSPECT-D: Towards modeling leaf optical properties through a complete lifecycle, Remote Sensing of Environment, 193, 204–215, https://doi.org/10.1016/j.rse.2017.03.004, 2017.

Krayenhoff, E. S., Christen, A., Martilli, A., and Oke, T. R.: A multi-layer radiation model for urban neighbourhoods with trees, Boundary-Layer Meteorology, 151, 139–178, https://doi.org/10.1007/s10546-013-9883-1, 2014.

Krayenhoff, E. S., Santiago, J.-L., Martilli, A., Christen, A., and Oke, T. R.: Parametrization of drag and turbulence for urban neighbourhoods with trees, Boundary-Layer Meteorology, 156, 157–189, https://doi.org/10.1007/s10546-015-0028-6, 2015.

Landier, L., Gastellu-Etchegorry, J.-P., Lauret, N., Yin, T., Malenovsky, Z., Al Bitar, A., Aval, J., Benhmida, S., Qi, J., and Zhang, X.: Calibration of urban canopies albedo and 3D shortwave radiative budget using remote-sensing data and the DART model, European Journal of Remote Sensing, 51, 739–753, https://doi.org/10.1080/22797254.2018.1462102, 2018.

Lam, S. K., Pitrou, A., and Seibert, S.: Numba: a LLVM-based Python JIT compiler, in: Proceedings of the Second Workshop on the LLVM Compiler Infrastructure in HPC, Austin, Texas, USA, 15 November 2015, 1–6, https://doi.org/10.1145/2833157.2833162, 2015.

https://doi.org/10.5194/egusphere-2026-5226
Preprint. Discussion started: 9 September 2026

Manni, M., Coccia, V., Nicolini, A., Marseglia, G., and Petrozzi, A.: Development and validation of a Monte Carlo-based numerical model for solar analyses in urban canyon configurations, Building and Environment, 170, 106638, https://doi.org/10.1016/j.buildenv.2019.106638, 2020.

Mei, S.-J., Chen, G., Wang, K., and Hang, J.: Parameterizing urban canopy radiation transfer using three-dimensional urban morphological parameters, Urban Climate, 60, 102363, https://doi.org/10.1016/j.uclim.2025.102363, 2025.

Mei, S.-J. and Sun, T.: URAY v1.0: a 3D Monte Carlo model for urban shortwave radiation [computer software], Zenodo, https://doi.org/10.5281/zenodo.22153465, 2026.

Meili, N., Manoli, G., Burlando, P., Bou-Zeid, E., Chow, W. T. L., Coutts, A. M., Roth, M., Velasco, E., Vivoni, E. R., and Fatichi, S.: An urban ecohydrological model to quantify the effect of vegetation on urban climate and hydrology (UT&C v1.0), Geoscientific Model Development, 13, 335–362, https://doi.org/10.5194/gmd-13-335-2020, 2020.

Menon, S., Akbari, H., Mahanama, S., Sednev, I., and Levinson, R.: Radiative forcing and temperature response to changes in urban albedos and associated CO2 offsets, Environmental Research Letters, 5, 014005, https://doi.org/10.1088/1748-9326/5/1/014005, 2010.

Overby, M., Willemsen, P., Bailey, B. N., Pardyjak, E. R., and Stoll, R.: A rapid and scalable radiation transfer model for complex urban domains, Urban Climate, 15, 25–44, https://doi.org/10.1016/j.uclim.2015.11.004, 2016.

Panao, M. J. N. O., Goncalves, H. J. P., and Ferrao, P. M. C.: A matrix approach coupled with Monte Carlo techniques for solving the net radiative balance of the urban block, Boundary-Layer Meteorology, 122, 217–241, https://doi.org/10.1007/s10546-006-9088-y, 2007.

Qin, Y.: Urban canyon albedo and its implication on the use of reflective cool pavements, Energy and Buildings, 96, 86–94, https://doi.org/10.1016/j.enbuild.2015.03.005, 2015.

Salvati, A., Kolokotroni, M., Kotopouleas, A., Watkins, R., Giridharan, R., and Nikolopoulou, M.: Impact of reflective materials on urban canyon albedo, outdoor and indoor microclimates, Building and Environment, 207, 108459, https://doi.org/10.1016/j.buildenv.2021.108459, 2022.

Sailor, D. J. and Fan, H.: Modeling the diurnal variability of effective albedo for cities, Atmospheric Environment, 36, 713–725, https://doi.org/10.1016/S1352-2310(01)00452-6, 2002.

Schoetter, R., Caliot, C., Chung, T.-Y., Hogan, R. J., and Masson, V.: Quantification of uncertainties of radiative transfer calculation in urban canopy models, Boundary-Layer Meteorology, 189, 103–138, https://doi.org/10.1007/s10546-023-00827-9, 2023.

Tolan, J., Yang, H. I., Nosarzewski, B., Couairon, G., Vo, H. V., Brandt, J., Spore, J., Majumdar, S., Haziza, D., Vamaraju, J., Moutakanni, T., et al.: Very high resolution canopy height maps from RGB imagery using self-supervised vision transformer and convolutional decoder trained on aerial lidar, Remote Sensing of Environment, 300, 113888, https://doi.org/10.1016/j.rse.2023.113888, 2024.

Trlica, A., Hutyra, L. R., Schaaf, C. L., Erb, A., and Wang, J. A.: Albedo, land cover, and daytime surface temperature variation across an urbanized landscape, Earth's Future, 5, 1084–1101, https://doi.org/10.1002/2017EF000569, 2017.

Villefranque, N., Hourdin, F., d'Alencon, L., Blanco, S., Boucher, O., Caliot, C., Coustet, C., Dauchet, J., El Hafi, M., Eymet, V., Farges, O., Forest, V., Fournier, R., Gautrais, J., Masson, V., Piaud, B., and Schoetter, R.: The "teapot in a city": A paradigm shift in urban climate modeling, Science Advances, 8, eabp8934, https://doi.org/10.1126/sciadv.abp8934, 2022.

Wang, C., Wang, Z.-H., and Ryu, Y.-H.: A single-layer urban canopy model with transmissive radiation exchange between trees and street canyons, Building and Environment, 191, 107593, https://doi.org/10.1016/j.buildenv.2021.107593, 2021.

Wang, L., Gastellu-Etchegorry, J.-P., Yin, T., Lauret, N., and Al Bitar, A.: 3D Monte Carlo surface-atmosphere radiative transfer modelling with DART, Remote Sensing of Environment, 303, 113946, https://doi.org/10.1016/j.rse.2023.113946, 2024.

https://doi.org/10.5194/egusphere-2026-5226
Preprint. Discussion started: 9 September 2026

Yang, J., Wang, Z.-H., and Kaloush, K. E.: Environmental impacts of reflective materials: Is high albedo a “silver bullet” for mitigating urban heat island?, Renewable and Sustainable Energy Reviews, 47, 830–843, https://doi.org/10.1016/j.rser.2015.03.092, 2015.

Yuan, C., Norford, L., and Ng, E.: A semi-empirical model for the effect of trees on the urban wind environment, Landscape and Urban Planning, 168, 84–93, https://doi.org/10.1016/j.landurbplan.2017.09.029, 2017.